Recent development of self-interaction-free time-dependent density-functional theory for nonperturbative treatment of atomic and molecular multiphoton processes in intense laser fields

Shih-I Chu

Articles you may be interested in

Strong field ionization rates simulated with time-dependent configuration interaction and an absorbing potential
J. Chem. Phys. **140**, 174113 (2014); 10.1063/1.4874156

A critical re-assignment of the Rydberg states of iodomethane based on new polarization data
J. Chem. Phys. **138**, 134308 (2013); 10.1063/1.4798972

Exact-exchange kernel of time-dependent density functional theory: Frequency dependence and photoabsorption spectra of atoms
J. Chem. Phys. **131**, 044110 (2009); 10.1063/1.3179756

A discrete time-dependent method for metastable atoms and molecules in intense fields
J. Chem. Phys. **120**, 10046 (2004); 10.1063/1.1735662

Self-interaction-free time-dependent density-functional theory for molecular multiphoton processes in intense laser fields
AIP Conf. Proc. **525**, 415 (2000); 10.1063/1.1291959

Recent development of self-interaction-free time-dependent density-functional theory for nonperturbative treatment of atomic and molecular multiphoton processes in intense laser fields

Shih-I Chu[a)]

Department of Chemistry, University of Kansas, and Kansas Center for Advanced Scientific Computing, Lawrence, Kansas 66045

In this paper, we present a short account of some recent developments of *self-interaction-free* density-functional theory (DFT) and time-dependent density-functional theory (TDDFT) for accurate and efficient treatment of the electronic structure, and time-dependent quantum dynamics of many-electron atomic and molecular systems. The conventional DFT calculations using approximate and explicit exchange-correlation energy functional contain spurious self-interaction energy and improper long-range asymptotic potential, preventing reliable treatment of the excited, resonance, and continuum states. We survey some recent developments of DFT/TDDFT with optimized effective potential (OEP) and self-interaction correction (SIC) for both atomic and molecular systems for overcoming some of the above mentioned difficulties. These DFT (TDDFT)/ OEP-SIC approaches allow the use of orbital-independent single-particle local potential which is self-interaction free. In addition we discuss several numerical techniques recently developed for efficient and high-precision treatment of the self-interaction-free DFT/TDDFT equations. The usefulness of these procedures is illustrated by a few case studies of atomic, molecular, and condensed matter processes of current interests, including (a) autoionizing resonances, (b) relativistic OEP-SIC treatment of atomic structure ($Z=2$–106), (c) shell-filling electronic structure in quantum dots, (d) atomic and molecular processes in intense laser fields, including multiphoton ionization, and very-high-order harmonic generation, etc. For the time-dependent processes, an alternative Floquet formulation of TDDFT is introduced for time-independent treatment of multiphoton processes in intense periodic or quasiperiodic fields. We conclude this paper with some open questions and perspectives of TDDFT. © 2005 American Institute of Physics. [DOI: 10.1063/1.1904587]

I. INTRODUCTION

In recent years, the density-functional theory (DFT) has become a widely used formalism for electron structure calculations of atoms, molecules, and solids.[1–6] The DFT is based on the earlier fundamental work of Hohenberg and Kohn[7] and Kohn and Sham.[8] In the Kohn–Sham DFT formalism,[8] the electron density is decomposed into a set of orbitals, leading to a set of one-electron Schrödinger-type equations to be solved self-consistently. The Kohn–Sham equations are structurally similar to the Hartree–Fock equations but include, in principle, exactly the *many-body* effects through a *local* exchange-correlation (xc) potential. Thus DFT is computationally much less expensive than the traditional *ab initio* many-electron wave-function approaches and this accounts for its great success for large systems. However, the DFT is well developed mainly for the *ground-state* properties only. The treatment of the *excited states* within the DFT is a more recent development.[9–15]

The essential element of DFT is the input of the *exchange-correlation* energy functional whose exact form is unknown. The simplest approximation for the xc-energy functional is through the *local spin-density approximation*[1,16] (LSDA) of homogeneous electronic gas. A deficiency of the LSDA is that the xc potential decays exponentially and does not follow the correct *long-range* asymptotic Coulombic ($-1/r$) behavior. As a result, the LSDA electrons are too weakly bound and for negative ions even unbound. More accurate forms of the xc-energy functionals are available from the *generalized gradient approximation* (GGA),[17–20] which takes into account the gradient of electron density. However, the xc potentials derived from these GGA energy functionals suffer similar problems like in LSDA and do not have the proper long-range asymptotic potential behavior either. Thus while the total energies of the ground states predicted by these GGA density functionals[17–20] are reasonably accurate, the excited-state energies and the ionization potentials obtained from the highest occupied orbital energies of atoms and molecules are not satisfactory, typically 30%–50% too low.[1,21] The problem of the incorrect long-range behavior of the LSDA and GGA energy functionals can be attributed to the existence of the *self-interaction energy*.[1,4,5,21,22] For proper treatment of atomic and molecular dynamics such as collisions or multiphoton ionization processes, etc., it is necessary that both the ionization potential and the excited-state properties be described more accurately. In addition, the

---

[a)]Electronic mail: sichu@ku.edu

treatment of time-dependent processes will require the use of time-dependent density-functional theory (TDDFT).

The TDDFT extends the concept of stationary DFT to time-dependent domain. For any interacting many-particle quantum system subject to a given time-dependent potential, all physical observables are uniquely determined by knowledge of the time-dependent density and the state of the system at any instant in time.[23,24] In particular, if the time-dependent potential is turned on at some time t_0 and the system has been in its ground state until t_0, all observables are unique functionals of the density only. In this case the initial state of the system at time t_0 will be a unique functional of the ground-state density itself, i.e., of the density at t_0. This unique relationship allows one to derive a computational scheme in which the effect of the particle-particle interaction is represented by a density-dependent single-particle potential, so that the time evolution of an interacting system can be investigated by solving a time-dependent auxiliary single-particle problem. Additional simplifications can be obtained in the linear response regime.[23–26] In the last several years there is considerable effort and success in the extension of the (weak-field) TDDFT and the use of linear response theory to the study of excitation energies,[27–31] frequency-dependent multipole polarizabilities,[26,32,33] optical spectra of molecules, clusters, and nanocrystals,[34,35] and autoionizing resonances,[21] etc.

The primary focus of this paper is to discuss some of the recent developments and applications of *self-interaction-free* TDDFT for the study of atomic and molecular multiphoton processes in intense laser fields. The strong-field atomic and molecular physics is one of the most active fields of forefront research in science and technology. The rapid advent of high-power and short-pulse laser technology in the last decade has facilitated the experimental exploration of multiphoton and very high-order ($>$300th order) nonlinear optical processes, leading to the discovery of a host of novel strong-field phenomena, such as multiphoton and above-threshold ionization of atoms, multiphoton and above-threshold dissociation of molecules, multiple high-order harmonic generation (HHG), chemical bond softening and hardening, Coulomb explosion, and coherent control of chemical and physical processes, etc. For the treatment of these strong-field processes, the conventional high-order perturbation approach is generally not adequate. On the other hand, nonperturbative approach using *ab initio* wave functions requires the solution of $(3N+1)$th-order time-dependent Schrödinger equation in space and time, where N is the number of electrons. But this is well beyond the capability of current computer technology for $N>2$. Even for the case of $N=2$, fully *ab initio* time-dependent study is still at the beginning stage. The single-active-electron (SAE) model[36,37] with frozen core is thus commonly used for describing the strong-field processes. However, within the SAE model, important physical phenomena such as excited-state resonances, dynamical response from individual valence spin orbital, inner core excitation, nonsequential ionization, and dynamical electron correlations, etc., cannot be treated. Clearly, a more complete formalism beyond the SAE and other phenomenological models is very desirable at this time for more comprehensive

and accurate treatment of atomic and molecular physics and chemical physics in strong fields.

We note, however, that the conventional (weak-field) TDDFT is not adequate for the treatment of strong-field processes. Similar to the stationary DFT case, due to the existence of the self-interaction energy, TDDFT calculations using *adiabatic* LDA or GGA energy functionals do not have the correct long-range asymptotic Coulombic ($-1/r$) potential. Moreover, nonperturbative framework for TDDFT will be required for the treatment of strong field processes. The recent development of self-interaction-free DFT and TDDFT removes some of these problems and provides powerful and practical nonperturbative frameworks for quantitative treatment of highly excited states and strong-field processes of many-electron quantum systems. A short account of these new developments and their applications will be discussed and examined in this paper.

In the following, we first briefly describe the self-interaction-free DFT for more accurate treatment of the electronic structure of atomic, molecular, and quantum dot systems. This is followed by a discussion of the self-interaction-free TDDFTs and associated computational techniques for *nonperturbative* treatment of multiphoton dynamics and very-high-order nonlinear optical processes in intense laser fields.

II. DFT WITH OPTIMIZED EFFECTIVE POTENTIAL AND SELF-INTERACTION CORRECTION

In the Kohn–Sham (KS) DFT formulation,[8] one solves the following set of one-electron Schrödinger-type equations for N-electron systems (in atomic units):

$$\hat{H}_{KS}\psi_{i\sigma}(\mathbf{r}) = \left[-\frac{1}{2}\nabla^2 + v_{\text{eff},\sigma}(\mathbf{r}) \right] \psi_{i\sigma}(\mathbf{r}) = \varepsilon_{i\sigma}\psi_{i\sigma}(\mathbf{r}),$$

$$(i = 1,2,\ldots,N_\sigma), \qquad (1)$$

where $v_{\text{eff},\sigma}(\mathbf{r})$ is the effective KS potential and σ is the spin index. The total density is given by

$$\rho(\mathbf{r}) = \sum_\sigma \sum_{i=1}^{N_\sigma} |\psi_{i\sigma}(\mathbf{r})|^2 = \rho_\uparrow(\mathbf{r}) + \rho_\downarrow(\mathbf{r}), \qquad (2)$$

and the ground-state wave function is determined by

$$\Psi = \frac{1}{\sqrt{N!}}\det[\psi_1\psi_2\cdots\psi_N]. \qquad (3)$$

The total energy of the ground state is obtained by the minimization of the Hohenberg–Kohn energy functional[7]

$$E[\rho_\uparrow,\rho_\downarrow] = T_s[\rho] + J[\rho] + E_{xc}[\rho_\uparrow,\rho_\downarrow] + \int v_{\text{ext}}(\mathbf{r})\rho(\mathbf{r})d\mathbf{r}.$$

$$(4)$$

Here T_s is the *noninteracting* KS kinetic energy,

$$T_s = \sum_\sigma \sum_{i=1}^{N_\sigma} \langle \psi_{i\sigma} | - \frac{1}{2}\nabla^2 | \psi_{i\sigma} \rangle, \tag{5}$$

$v_{\text{ext}}(\mathbf{r})$ is the "external" potential due to the electron-nucleus interaction, $J[\rho]$ is the classical electron-electron repulsive energy,

$$J[\rho] = \frac{1}{2} \int \int \frac{\rho(\mathbf{r})\rho(\mathbf{r}')}{|\mathbf{r}-\mathbf{r}'|} d\mathbf{r}\, d\mathbf{r}', \tag{6}$$

and $E_{\text{xc}}[\rho_\uparrow, \rho_\downarrow]$ is the xc-energy functional. Minimization of the total energy functional, Eq. (4), subject to the constraint

$$\int \rho_\sigma(\mathbf{r}) d\mathbf{r} = N_\sigma, \tag{7}$$

gives rise to the KS equations (1) with the effective potential

$$v_{\text{eff},\sigma}(\mathbf{r}) = v_{\text{ext}}(\mathbf{r}) + \frac{\delta J[\rho]}{\delta\rho_\sigma(r)} + \frac{\delta E_{\text{xc}}[\rho_\uparrow, \rho_\downarrow]}{\delta\rho_\sigma(\mathbf{r})}$$

$$= v_{\text{ext}}(\mathbf{r}) + \int \frac{\rho(\mathbf{r}')}{|\mathbf{r}-\mathbf{r}'|} d\mathbf{r}' + v_{\text{xc},\sigma}(\mathbf{r}), \tag{8}$$

where $v_{\text{xc},\sigma}(\mathbf{r})$ is the exchange-correlation potential,

$$v_{\text{xc},\sigma}(\mathbf{r}) = \frac{\delta E_{\text{xc}}[\rho_\uparrow, \rho_\downarrow]}{\delta\rho_\sigma(\mathbf{r})}. \tag{9}$$

The KS equations are to be solved self-consistently, starting from some initial estimate of the density $\rho_\sigma(\mathbf{r})$, until convergence is reached. In actual calculations, the KS Hamiltonian in Eq. (4) must be fixed by a particular choice of the xc-energy functional, $E_{\text{xc}}[\rho_\uparrow, \rho_\downarrow]$. However, both LSDA and GGA energy functional forms contain spurious self-interaction contributions. Such self-interaction contribution can be seen from Eq. (4), where the two terms $J[\rho]$ and $E_{\text{xc}}[\rho_\uparrow, \rho_\downarrow]$ should, in principle, cancel each other exactly in the limit of one-electron system, if the exact form for $E_{\text{xc}}[\rho_\uparrow, \rho_\downarrow]$ is used. In practice, $E_{\text{xc}}[\rho_\uparrow, \rho_\downarrow]$ needs to be approximated, leading to the self-interaction energy. The existence of such self-interaction energy is the main source of error responsible for the incorrect *long-range* behavior of the exchange-correlation potential $v_{\text{xc},\sigma}(\mathbf{r})$. Thus the elimination of the self-interaction contribution is essential for the proper treatment of the ionization potentials and excited-state properties.

In the last several years, considerable attention has been paid to the methodology for the removing of self-interaction energy. One approach for improving $E_{\text{xc}}[\rho_\uparrow, \rho_\downarrow]$ is based on the generalization of the so-called *optimized effective potential* (OEP) formalism.[38,39] In this approach, one solves a set of one-electron equations, similar to the KS equations in Eq. (1),

$$\hat{H}_{\text{OEP}} \phi_{i\sigma}(\mathbf{r}) = \left[-\frac{1}{2}\nabla^2 + V_\sigma^{\text{OEP}}(\mathbf{r}) \right] \phi_{i\sigma}(\mathbf{r}) = \varepsilon_{i\sigma} \phi_{i\sigma}(\mathbf{r}),$$

$$(i = 1, 2, \ldots, N_\sigma). \tag{10}$$

The optimized effective potential $V_\sigma^{\text{OEP}}(\mathbf{r})$ is obtained by the requirement that the spin orbitals $\{\phi_{i\sigma}\}$ in Eq. (10) are those that minimize the total energy functional $E[\{\phi_{i\uparrow}, \phi_{j\downarrow}\}]$,

$$\frac{\delta E^{\text{OEP}}[\{\phi_{i\uparrow}, \phi_{j\downarrow}\}]}{\delta V_\sigma^{\text{OEP}}(\mathbf{r})} = 0, \tag{11}$$

where

$$E^{\text{OEP}}[\{\phi_{i\uparrow}, \phi_{j\downarrow}\}] = T_s[\{\phi_{i\uparrow}, \phi_{j\downarrow}\}] + J[\{\phi_{i\uparrow}, \phi_{j\downarrow}\}]$$

$$+ E_{\text{xc}}[\{\phi_{i\uparrow}, \phi_{j\downarrow}\}] + \int v_{\text{ext}}(\mathbf{r})\rho(\mathbf{r}) d\mathbf{r}. \tag{12}$$

Equation (11) can be written as, using the chain rule for functional derivative,

$$\sum_j \int d\mathbf{r}' \frac{\delta E^{\text{OEP}}[\{\{\phi_{i\uparrow}, \phi_{i'\downarrow}\}\}]}{\delta\phi_{j\sigma}(\mathbf{r}')} \cdot \frac{\delta\phi_{j\sigma}(\mathbf{r}')}{\delta V_\sigma^{\text{OEP}}(\mathbf{r})} + \text{c.c.} = 0. \tag{13}$$

While the physical idea of the OEP method is simple and appealing, Eq. (13) leads to an integral equation which is computationally impractical to solve. Recently, Krieger, Li, and Iafrate[40] (KLI) have worked out an approximate, albeit accurate, procedure to circumvent this difficulty, reducing the determination of V_σ^{OEP} to the solution of simple linear equations. In all the earlier KLI calculations so far,[5,40] however, the exchange part of the density functional contains Hartree–Fock-type potential. While such a procedure provides accurate results for the exchange part of E_{xc} it is computationally more expensive than the traditional DFT calculations where only single-particle *local* potential is used. Thus it is desirable to explore an approximate and yet accurate procedure within the KLI framework involving only the use of local potentials. This would greatly speed up the computations of the static and dynamical properties of many-electron systems. As will be shown below, the self-interaction-correction (SIC) procedure, similar to the original KLI method, allows also the construction of self-interaction-free effective potential which is local and orbital independent Further, the OEP so constructed, denoted by $V_{\text{KLI},\sigma}^{\text{SIC}}(\mathbf{r})$ below, has the proper long-range asymptotic ($-1/r$) behavior and thus is suitable for the determination of both ground- and excited-state properties of many-electron systems.

We shall adopt the following total energy functional with *explicit* SIC form[21,22,41]

$$E_{\text{SIC}}^{\text{OEP}}[\{\phi_{i\uparrow}, \phi_{j\downarrow}\}] = E^{\text{OEP}}[\{\phi_{i\uparrow}, \phi_{j\downarrow}\}]$$

$$- \sum_\sigma \sum_i \{J[\rho_{i\sigma}] + E_{\text{xc}}[\rho_{i\sigma}, 0]\}, \tag{14}$$

where $E^{\text{OEP}}[\{\phi_{i\uparrow}, \phi_{j\downarrow}\}]$ is given in Eq. (12). Extending the OEP-KLI procedure, we arrive at

$$V_{\text{SIC},\sigma}^{\text{OEP}}(\mathbf{r}) = v_{\text{ex}}(\mathbf{r}) + \int \frac{\rho(\mathbf{r}')}{|\mathbf{r}-\mathbf{r}'|} d\mathbf{r}' + \frac{\delta E_{\text{xc}}[\rho_\uparrow, \rho_\downarrow]}{\delta\rho_\sigma(\mathbf{r})}$$

$$+ V_{\text{SIC},\sigma}(\mathbf{r}), \tag{15}$$

where

$$V_{\text{SIC},\sigma}(\mathbf{r}) = \sum_i \frac{\rho_{i\sigma}(\mathbf{r})}{\rho_\sigma(\mathbf{r})} \{v_{i\sigma}(\mathbf{r}) [\bar{V}_{\text{SIC},\sigma}^i - \bar{v}_{i\sigma}]\}, \tag{16}$$

TABLE I. The ionization potentials (in atomic units) of ground states of neutral atoms ($Z \leq 18$) calculated from the highest occupied orbital energies by various exchange-correlation energy functionals.

Atom	Non-KLI-SIC		KLI-SIC		
	xLSDA	BLYP	xLSDA	BLYP	Expt.[a]
He	0.517	0.585	0.918	0.950	0.904
Li	0.100	0.111	0.196	0.194	0.198
Be	0.170	0.201	0.308	0.323	0.343
B	0.120	0.143	0.290	0.304	0.305
C	0.196	0.218	0.412	0.422	0.414
N	0.276	0.297	0.536	0.543	0.534
O	0.210	0.266	0.479	0.523	0.501
F	0.326	0.377	0.645	0.680	0.640
Ne	0.443	0.492	0.808	0.837	0.793
Na	0.097	0.107	0.187	0.184	0.189
Mg	0.142	0.168	0.256	0.267	0.281
Al	0.086	0.102	0.192	0.198	0.217
Si	0.144	0.160	0.275	0.279	0.300
P	0.203	0.219	0.358	0.361	0.385
S	0.174	0.219	0.344	0.375	0.381
Cl	0.254	0.295	0.447	0.472	0.477
Ar	0.334	0.373	0.549	0.571	0.579

[a]Reference 104.

$$v_{i\sigma}(\mathbf{r}) = -\int \frac{\rho_{i\sigma}(\mathbf{r}')}{|\mathbf{r} - \mathbf{r}'|} d\mathbf{r}' - \frac{\delta E_{xc}[\rho_{i\sigma}, 0]}{\delta \rho_{i\sigma}(\mathbf{r})}, \tag{17}$$

and

$$\bar{V}_{SIC,\sigma}^{i} = \langle \phi_{i\sigma} | V_{SIC,\sigma}(\mathbf{r}) | \phi_{i\sigma} \rangle, \tag{18}$$

$$\bar{v}_{i\sigma} = \langle \phi_{i\sigma} | v_{i\sigma}(\mathbf{r}) | \phi_{i\sigma} \rangle. \tag{19}$$

The set of OEP equations in Eq. (10), with $V_{\sigma}^{OEP}(r)$ replaced by local potential $V_{SIC,\sigma}^{OEP}(\mathbf{r})$ in Eq. (15), is to be solved self-consistently. Finally, one can choose $\bar{V}_{SIC,\sigma}^{i=N_\sigma} = \bar{v}_{N\sigma}$ for the highest occupied orbital as suggested by the KLI procedure. The energy of the highest occupied orbital provides an approximate value for the first ionization potential.[42] In the following we discuss some recent applications of the OEP/KLI-SIC procedure to the atomic and quantum dot electronic structure calculations.

A. Nonrelativistic atomic structure calculations

The OEP/KLI-SIC method described above has been recently applied to the calculation of total energies and ionization potentials for neutral atoms and negative ions ($Z=2$–18).[21] Table I shows some representative results of the OEP/KLI-SIC calculations for the ionization potentials of neutral atoms. It is seen that while the ionization potentials from the DFT calculations using the LSDA and Becke-Lee-Yang-Parr (BLYP) functionals have 30%–50% discrepancy from the exact results, the corresponding results after the KLI-SIC procedure are markedly improved to within 1%–5% of the exact values. To understand the physical origin of such an improvement, we show in Fig. 1 the effective potential $rV_{eff}(r)$ of LSDA and BLYP with and without KLI-SIC for the Ne atom. Notice that both LSDA and BLYP potentials (without KLI-SIC) give rise to wrong

long-range behavior [$rV_{eff}(r) \to 0$ asymptotically]. On the other hand, the corresponding potentials with KLI-SIC reproduce the correct asymptotic behavior, namely, $rV_{eff}(r) \to -1$. This correct long-range behavior is crucial for proper DFT treatment of excited and continuum states as well as the autoionizing resonances to be described next.

B. Autoionizing resonances

Because of the lack of proper long-range interaction behavior, previous photoionization calculations of complex atoms using LSDA or GGA energy functionals fail to exhibit the excited-state structure such as the prominent *autoionizing resonances*.[25,26] Using the OEP/KLI-SIC procedure,[21] we have recently performed a calculation of the photoionization spectrum of Ne using time-dependent LSDA (within linear response theory). It is seen that the time-dependent LSDA (with KLI-SIC) results agree well with the experimental data in the broad peak region (Fig. 2), followed by a series of sharp resonances due to $2s \to np$ resonance transitions[21] (Fig. 3). The calculated linewidths and resonance line profile parameters are also in good agreement with both
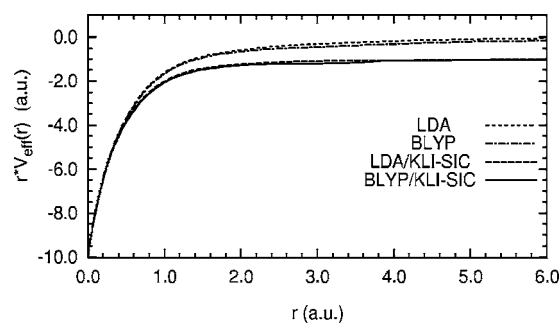

FIG. 1. The one-electron effective potentials $r \cdot V_{eff}(r)$ of LSDA and BLYP with and without the KLI-SIC for Ne atom.
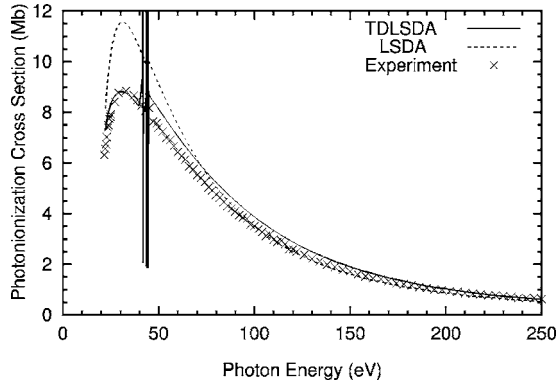
FIG. 2. The total photoionization cross sections of time-independent and time-dependent calculations with LSDA/KLI-SIC potential.

experimental[43] and configuration-interaction (R-matrix) (Ref. 44) results. (We note that in the photoionizations,[21] two values of the $2s$ orbital energy are used in the linear response calculations, one taken directly from the OEP/KLI-SIC data and the other from the experimental value. Both calculations give rise to nearly identical autoionizing spectrum except the resonance positions are slightly shifted.) To our knowledge this is the first successful DFT calculation which produces the fine structure of *autoionizing resonances* of complex atoms.

C. Relativistic DFT calculations of atomic structure (Z=2–106)

The *relativistic* density-functional theory (RDFT) is the generalization of the nonrelativistic Hohenberg–Kohn–Sham density-functional formalism[7,8] to the relativistic regime.[45,46] When the many-body effects are approximated locally as being those of a relativistic homogeneous electron gas, the relativistic local density approximation is obtained.[45,46]

In the RDFT, one solves the following single-particle Dirac–Fock-type equation for N-electron atomic systems (in atomic units)

$$[c\alpha \cdot \mathbf{p} + \beta c^2 + \nu_{\text{eff},\sigma}(\mathbf{r})]\psi_{i\sigma} = \epsilon_{i\sigma}\psi_{i\sigma}(\mathbf{r}), \quad i = 1, 2, \ldots, N_\sigma \tag{20}$$

where $\nu_{\text{eff},\sigma}$ is the effective one-particle local potential, σ is the spin index, and $\{\psi_{i\sigma}\}$ are the four-component spinors. The total electron density is given by
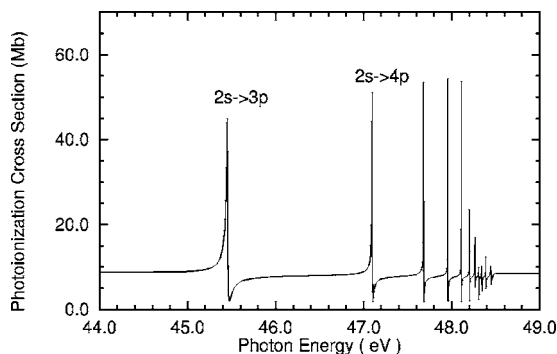

FIG. 3. The photoionization cross sections near the $2s\rightarrow np$ resonant transitions, showing the autoionizing resonance profiles. The results are obtained by the TDLSDA with KLI-SIC potential. The experimental value of the $2s$ orbital energy is used in the calculation.

$$\rho = \sum_\sigma \sum_{i=1}^{N_\sigma} \psi_{i\sigma}^+(\mathbf{r})\psi_{i\sigma}(\mathbf{r}) = \sum_\sigma \sum_{i=1}^{N_\sigma} \rho_{i\sigma}(\mathbf{r}), \tag{21}$$

and the total energy of the ground state is expressed as

$$E[\rho] = T_s[\rho] + J[\rho] + E_{\text{xc}}[\rho_\uparrow, \rho_\downarrow] + \int \nu_{\text{ext}}(\mathbf{r})\rho(\mathbf{r})d\mathbf{r}. \tag{22}$$

Here T_s is the kinetic energy of the noninteracting N-electron systems including the rest-mass energy,

$$T_s = \sum_\sigma \sum_{i=1}^{N_\sigma} \langle \psi_{i\sigma} | c\alpha \cdot \mathbf{p} + \beta c^2 | \psi_{i\sigma} \rangle, \tag{23}$$

E_{xc} is the relativistic counterpart of the exchange-correlation energy, and v_{ext} is the external potential including the electron-nucleus interaction. The effective potential in Eq. (20) is given by

$$\nu_{\text{eff},\sigma}(\mathbf{r}) = v_{\text{ext}}(\mathbf{r}) + \int \frac{\rho(\mathbf{r}')}{|\mathbf{r} - \mathbf{r}'|}d\mathbf{r}' + v_{\text{xc},\sigma}(\mathbf{r}), \tag{24}$$

where $\nu_{\text{xc},\sigma}$ is the relativistic exchange-correlation (xc) potential,

$$v_{\text{xc},\sigma}(\mathbf{r}) = \frac{\delta E_{\text{xc}}[\rho_\uparrow, \rho_\downarrow]}{\delta \rho_\sigma(\mathbf{r})}. \tag{25}$$

Similar to the nonrelativistic case, the RDFT described above contains the undesirable self-interaction energy. Thus the relativistic xc potential[45–47] does not have the proper long-range behavior either. To overcome such problems, a self-interaction-free relativistic DFT has been developed, based on the extension of the nonrelativistic OEP/KLI-SIC formalism to the relativistic domain.[48]

Using the relativistic OEP/KLI-SIC formalism, a detailed atomic structure calculation of the orbital binding energies and ionization potentials (obtained from the highest occupied orbital energies) is performed for the ground states of atoms with nuclear charge Z=2–106.[48] The results are in good agreement with the experimental data to within a few percent (Fig. 4) across the periodic table (Z=2–106). Figure 4 shows that the inclusion of the relativistic correlation energy functional[48] leads to significant improvement of the results, particularly for the high-Z atoms. We note that Eq. (1) or Eq. (20) can be solved accurately and efficiently by means of the *generalized pseudospectral* (GPS) technique[49,50] which allows *nonuniform* and optimal spatial discretization of the Kohn–Sham Hamiltonian with the use of only a modest number of grid points.[21,48]

D. Electronic structure of quantum dots

Recent advances in semiconductor technology have led to the fabrication of zero-dimensional structure called *quantum dots*.[51,52] A recent measurement by Tarucha *et al.*[53] has probed the electronic structure of quantum dots through single-electron tunneling spectroscopy. An instructive finding is the existence of *shell* structure of addition energies. The addition energy $\mu(N)$ is defined to be the energy needed to add an electron into $(N-1)$ electron system, namely, $\mu(N) = E_{\text{tot}}(N) - E_{\text{tot}}(N-1)$, where, $E_{\text{tot}}(N)$ is the total energy of the
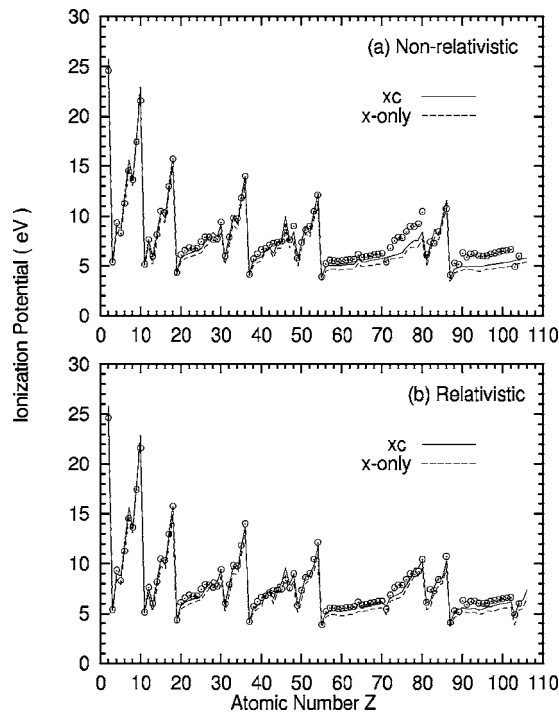
FIG. 4. Ionization potentials calculated by (a) nonrelativistic OEP/KLI-SIC and (b) relativistic OEP/KLI-SIC with exchange only (dashed line) and xc (solid line)-energy functionals for neutral atoms with $2 \leqslant Z \leqslant 106$. The experimental ionization potentials are also presented (open circle) for comparison.

N-electron quantum dot. Several recent theoretical studies have explored the shell-filling behavior of a few-electron (less than 20) quantum dots using the conventional LSDA or GGA energy functional,[54–56] but no detailed exploration has been performed on the general shell-filling behavior of many-electron quantum dots. In a recent study, we extended the OEP/KLI-SIC formalism to the study of the electronic structure and shell-filling behavior of quantum dots with $N = 2-60$.[57]

Figure 5 shows the *capacitive energy*, $\mu(N) - \mu(N-1)$, as a function of the electronic number N calculated by the BLYP (solid line) and BLYP/KLI-SIC (dashed line) proce-
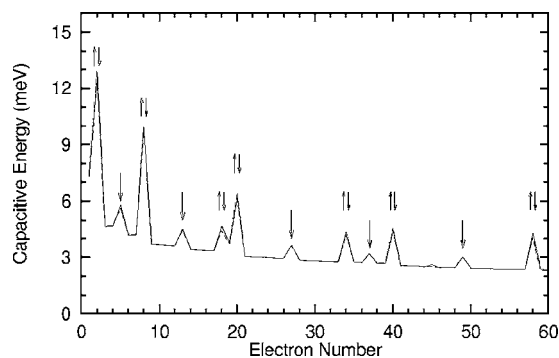

FIG. 5. Capacitive energies $[\mu(N) - \mu(N-1)]$ of N-electron quantum dots confined by a spherical harmonic potential ($\omega = 0.75$), exhibiting the shell-filling structure. Both BLYP and BLYP/KLI-SIC procedures are used in the DFT calculation. Solid line corresponds to the BLYP results where $\mu(N) = E_{\text{tot}}(N) - E_{\text{tot}}(N-1)$ is adopted. The dashed line shows the BLYP/KLI-SIC results where $\mu(N)$ is taken directly from the highest occupied orbital energy.

dures, exhibiting the detailed shell and subshell electronic structure of *many-electron* quantum dots. We note that although numerical values of the capacitive energies differ by a few percent, all the methods (LSDA, LSDA/KLI-SIC, BLYP, BLYP/KLI-SIC) used in the calculations[57] lead to the same shell and subshell structure patterns. To understand the origin of the *shell-filling* structure, we first examine the energy order of individual electron orbital. Using this energy ordering, one can identify all the shell structures in Fig. 5. For example, those peak positions marked ↑↓ correspond to the quantum dots with filled shells or subshells. The most prominent shell structure occurs at the following "magic" numbers $N = 2(1s^2)$, $8(1s^2sp^6)$, $20(1s^22p^63d^{10}2s^2)$, $40(1s^22p^63d^{10}2s^24f^{14}3p^6)$, etc., corresponding to the fully occupied shells. The smaller peaks marked ↓ in Fig. 5 can also be identified as those quantum dots with *half-filled* subshells. It is instructive to see that the Hund's rule is also applicable to the quantum dot systems here.[57]

III. RECENT DEVELOPMENT OF SELF-INTERACTION-FREE TDDFT FOR NONPERTURBATIVE TREATMENT OF ATOMIC MULTIPHOTON PROCESSES IN INTENSE LASER FIELDS

The TDDFT as a rigorous formalism is a more recent development in DFT, although the historical roots date back to the time-dependent Thomas–Fermi model proposed by Bloch in 1933.[58] The central result of modern TDDFT is a set of time-dependent Kohn–Sham (TDKS) equations which are structurally similar to the time-dependent Hartree–Fock (TDHF) equations but include (in principle, exactly) all many-body effects through a local time-dependent xc potential.[23,24] To date, most applications of TDDFT fall in the regime of *weak-field* linear or nonlinear response and the adiabatic LSDA energy functional is often used.[23,25,26,59] Applications of the time-dependent LSDA approach have been made to the photoresponse of atoms, molecules, clusters, nanocrystals, semiconductor surfaces, and bulk semiconductor in the weak-field perturbative regime.[25,26,34,35,59]

As indicated in the Introduction, the conventional (weak-field) TDKS formalism cannot be directly applied to the study of multiphoton processes in *intense* laser fields. In this section, we discuss a TDDFT with OEP and SIC for nonperturbative treatment of many-electron quantum systems in intense laser fields,[60] based on the extension of the *steady-state* OEP/KLI-SIC procedure[21] to the time domain. We note that a related TDOEP-KLI method without the use of SIC was proposed by Ullrich and Gross.[61] The latter method provides an accurate procedure for the calculation of the exchange part of the time-dependent potential. But computationally it can be more time consuming than the conventional TDKS approach since the TDOEP-KLI procedure requires the construction of Hartree–Fock-type potential at each time step. The advantage of the TDOEP/KLI-SIC approach[60] is that it allows the construction of self-interaction-free time-dependent local OEP which is also orbital independent. This greatly facilitates the study of time-dependent processes of many-electron quantum systems in strong fields.

A. TDDFT with OEP/KLI-SIC for atomic multiphoton processes in intense pulsed laser fields

The quantum mechanical *action* of a many-electron system interacting with an external field can be expressed as[60,61]

$$A[\{\psi_{i\sigma}\}] = \sum_\sigma \sum_i \int_{-\infty}^{t_1} dt \int \psi_{i\sigma}^*(\mathbf{r},t)\left(i\frac{\partial}{\partial t} + \frac{\nabla^2}{2}\right)$$

$$\times \psi_{i\sigma}(\mathbf{r},t)d\mathbf{r} - \sum_\sigma \int_{-\infty}^{t_1} dt \int \rho_\sigma(\mathbf{r},t)v_{\text{ext}}(\mathbf{r},t)d\mathbf{r}$$

$$- \frac{1}{2}\int_{-\infty}^{t_1} dt \int\int \frac{\rho_\sigma(\mathbf{r},t)\rho_\sigma(\mathbf{r}',t)}{|\mathbf{r}-\mathbf{r}'|}d\mathbf{r}\,d\mathbf{r}'$$

$$- A_{\text{xc}}[\{\psi_{i\sigma}\}], \tag{26}$$

where $\{\psi_{i\sigma}(\mathbf{r},t)\}$ are the time-dependent spin orbitals, $N = \Sigma_\sigma N_\sigma$ is the total number of electrons, $v_{\text{ext}}(\mathbf{r},t)$ is the external potential which includes the electron-nucleus Coulomb interaction and the coupling of the electron to the external laser fields, $\rho(\mathbf{r},t) = \Sigma_\sigma \rho_\sigma(\mathbf{r},t)$ is the total electron density with the spin density

$$\rho_\sigma(\mathbf{r},t) = \sum_i^{N_\sigma} \psi_{i\sigma}^*(\mathbf{r},t)\psi_{i\sigma}(\mathbf{r},t), \tag{27}$$

and $A_{\text{xc}}[\{\psi_{i\sigma}\}]$ is the xc action functional. The spin orbitals satisfy the one-electron Schrödinger-type equation,

$$i\frac{\partial}{\partial t}\psi_{i\sigma}(\mathbf{r},t) = \left(-\frac{1}{2}\nabla^2 + V_\sigma(\mathbf{r},t)\right)\psi_{i\sigma}(\mathbf{r},t), \tag{28}$$

where $V_\sigma(\mathbf{r},t)$ will be the TDOEP if we choose the set of spin orbitals $\{\psi_{i\sigma}\}$ which render the total action functional $A[\{\psi_{i\sigma}\}]$ *stationary*:

$$\frac{\delta A[\{\psi_{i\sigma}\}]}{\delta V_\sigma(\mathbf{r},t)} = 0. \tag{29}$$

Following a procedure similar to the TDOEP/KLI scheme,[61] one obtains the following general expression for the time-dependent xc potential:

$$V_{\text{xc},\sigma}(\mathbf{r},t) = \sum_i \frac{\rho_{i\sigma}(\mathbf{r},t)}{\rho_\sigma(\mathbf{r},t)}\frac{1}{2}\{v_{i\sigma}(\mathbf{r},t) + v_{i\sigma}^*(\mathbf{r},t)\}$$

$$+ \sum_i \frac{\rho_{i\sigma}(\mathbf{r},t)}{\rho_\sigma(\mathbf{r},t)}\left\{\bar{V}_{\text{xc},i\sigma} - \frac{1}{2}[\bar{v}_{i\sigma} + \bar{v}_{i\sigma}^*]\right\}$$

$$+ \frac{i}{4\rho_\sigma(\mathbf{r},t)}\sum_i \nabla^2\rho_{i\sigma}(\mathbf{r},t)$$

$$\times \int_{-\infty}^t dt'[\bar{v}_{i\sigma}(t') - \bar{v}_{i\sigma}^*(t')], \tag{30}$$

where the last term contains the memory effect and

$$v_{i\sigma}(\mathbf{r},t) = \frac{\delta A_{\text{xc}}}{\psi_{i\sigma}^*\delta\psi_{i\sigma}}, \quad v_{i\sigma}^*(\mathbf{r},t) = \frac{\delta A_{\text{xc}}}{\psi_{i\sigma}\delta\psi_{i\sigma}^*}. \tag{31}$$

If we use the following explicit SIC expression for the xc action functional,[60]

$$A_{\text{xc}}[\{\psi_{i\sigma}\}] = \int_{-\infty}^{t_1} dt E_{\text{xc}}[\rho_\uparrow(\mathbf{r},t),\rho_\downarrow(\mathbf{r},t)]$$

$$- \sum_\sigma \sum_{i=1}^{N_\sigma} \int_{-\infty}^{t_1} dt\{J[\rho_{i\sigma}] + E_{\text{xc}}[\rho_{i\sigma},0]\}, \tag{32}$$

where E_{xc} is the adiabatic time-dependent xc energy functional, we obtain

$$v_{i\sigma}(\mathbf{r},t) = v_{i\sigma}^*(\mathbf{r},t) = \frac{\delta E_{\text{xc}}^{\text{SIC}}}{\delta\rho_{i\sigma}}. \tag{33}$$

Note that $v_{i\sigma}$ is now a real function of $\mathbf{r}$ and t. Thus the memory term in Eq. (30) vanishes identically. Similar results are obtained as long as one uses an explicit E_{xc} form (such as that in LSDA or GGA) of energy functional and the adiabatic approximation.

The use of the SIC form in Eq. (32) removes the spurious self-interaction terms in conventional TDDFT and results in a proper long-range asymptotic potential. Another major advantage of this procedure is that only local potential is required to construct the *orbital-independent* OEP. This facilitates considerably the numerical computation.

By extending the steady-state OEP/KLI-SIC procedure[21] to the time-dependent domain, we obtain the time-dependent (TD) OEP as

$$V_\sigma(\mathbf{r},t) = v_{\text{ext}}(\mathbf{r},t) + \frac{\delta J[\rho]}{\delta\rho_\sigma(\mathbf{r},t)} + V_{\text{SIC},\sigma}(\mathbf{r},t), \tag{34}$$

where

$$V_{\text{SIC},\sigma}(\mathbf{r},t) = \sum_i \frac{\rho_{i\sigma}(\mathbf{r},t)}{\rho_\sigma(\mathbf{r},t)}\{v_{i\sigma}(\mathbf{r},t) + [\bar{V}_{\text{SIC},\sigma}^i(t) - \bar{v}_{i\sigma}(t)]\}, \tag{35}$$

$$v_{i\sigma}(\mathbf{r},t) = \frac{\delta E_{\text{xc}}[\rho_\uparrow(\mathbf{r},t),\rho_\downarrow(\mathbf{r},t)]}{\delta\rho_\sigma(\mathbf{r},t)} - \frac{\delta J[\rho_{i\sigma}(\mathbf{r},t)]}{\delta\rho_{i\sigma}(\mathbf{r},t)}$$

$$- \frac{\delta E_{\text{xc}}[\rho_{i\sigma}(\mathbf{r},t),0]}{\delta\rho_{i\sigma}(\mathbf{r},t)}, \tag{36}$$

and

$$\bar{V}_{\text{SIC},\sigma}^i(t) = \langle\psi_{i\sigma}|V_{\text{SIC},\sigma}(\mathbf{r},t)|\psi_{i\sigma}\rangle, \tag{37}$$

$$\bar{v}_{i\sigma}(t) = \langle\psi_{i\sigma}|v_{i\sigma}(\mathbf{r},t)|\psi_{i\sigma}\rangle. \tag{38}$$

Equations (28) and (34) are to be solved self-consistently. Note that since the exact form of $v_{\text{xc}\sigma}(\mathbf{r},t)$ is unknown, the adiabatic approximation is often used in the TDDFT calculations:

$$v_{\text{xc}\sigma}(\mathbf{r},t) = v_{\text{xc}\sigma}[\rho_\sigma]|_{\rho_\sigma=\rho\sigma(\mathbf{r},t)}. \tag{39}$$

Finally Eq. (28) is an initial value problem and the initial wave function can be determined by

$$\psi_{i\sigma}(\mathbf{r},t)_{t=0} = \phi_{i\sigma}(\mathbf{r})\cdot e^{-i\epsilon_{i\sigma}t}|_{t=0}, \tag{40}$$

where $\phi_{i\sigma}(\mathbf{r})$ and $\epsilon_{i\sigma}$ are the eigenfunction and eigenvalue of the time-independent Kohn–Sham equation (with OEP/KLI-SIC) for the static case.[21]

B. Time-dependent generalized pseudospectral method for numerical solution of self-interaction-free TDDFT equations

In this section we briefly describe a numerical procedure recently developed for accurate and efficient solution of the time-dependent OEP/SIC equation, Eq. (28). The commonly used procedures for the time propagation of the Schrödinger or TDDFT equation employ *equal-spacing* spatial grid discretization.[62–65] For processes such as HHG, accurate time-dependent wave functions are required to achieve convergence since the intensity of various harmonic peaks can span a range of many (10–20) orders of magnitude. High-precision wave functions are, however, more difficult to achieve by the conventional equal-spacing spatial-grid-discretization time-dependent techniques, due to the Coulomb singularity at the origin and the long-range behavior of the Coulomb potential. To achieve more accurate wave-function propagation, a numerical procedure, the *time-dependent generalized pseudospectral* (TDGPS) method[66] has been recently introduced. The TDGPS procedure consists of the following two basic elements: (i) The GPS technique[49,50] is used for *nonuniform* optimal grid discretization of the radial coordinates and the Hamiltonian. It has been shown that the number of grid points required in the GPS procedure can be orders of magnitude smaller than those used by the conventional equal-spacing discretization methods. Yet considerably higher accuracy in wave functions and therefore HHG spectra can be achieved since the physically more important short-range regime is more accurately treated by the TDGPS method.[66] (ii) A split-operator technique in the *energy* representation is introduced for efficient time propagation of the wave functions. More detailed discussion of the TDGPS method is given in a later molecular section.

C. Multiphoton quantum dynamics of atomic systems in intense laser fields

In this section we discuss several recent applications of the TDOEP/KLI-SIC formalism to the nonperturbative study of multiphoton processes of many-electron atomic systems in intense laser fields, focused particularly on the phenomenon of *multiple* HHG in intense laser fields. The study of the HHG phenomena is one of the most rapidly developing topics in strong-field atomic and molecular physics.[36,67–73] The generation of harmonic orders well in excess of 100 from noble gas, diatomic and polyatomic molecules, and cluster targets has been demonstrated by several recent experiments.[68–72] For example, in a recent experiment,[71] ultrashort laser pulses (with 26 fs pulse duration) from a Ti:sapphire laser have been used to generate coherent radiation at wavelengths as short as 2.7 nm (460 eV). These wavelengths are well within the "water window" region of x-ray transmission. Thus the HHG mechanism provides a simple and powerful new route to generate coherent x-ray laser source which is technically much less demanding and less energy intensive than current plasma based x-ray schemes. The availability of such a *compact* laboratory (*table-top*) system for the generation of coherent x rays holds

promise as a source for biological holography and nonlinear optics in the x-ray regime. Another potential new application of HHG processes is the possibility of generating laser pulses of *ultrashort* duration (tens of attoseconds) in the near future, leading a way to perform *attosecond* spectroscopy and study new dynamical phenomena with attosecond time resolution.

To study HHG, we start from the calculation of the total induced dipole moment and dipole acceleration of N-electron systems which can be expressed in terms of electron density ρ as follows:

$$d(t) = \int \rho(\mathbf{r},t)z\,d\mathbf{r} = \sum_{i\sigma} \langle \psi_{i\sigma}(\mathbf{r},t)|z|\psi_{i\sigma}(\mathbf{r},t)\rangle, \qquad (41)$$

$$d_A(t) = \int \rho(\mathbf{r},t)\frac{d^2z}{dt^2}d\mathbf{r}$$

$$= -\sum_{i\sigma} \langle \psi_{i\sigma}(\mathbf{r},t)|\frac{\partial V_{\mathrm{eff},\sigma}([\rho];\mathbf{r},t)}{\partial z}|\psi_{i\sigma}(\mathbf{r},t)\rangle$$

$$+ \sum_{i\sigma} \langle \psi_{i\sigma}(\mathbf{r},t)|\frac{\mathbf{E}(t)\cdot\mathbf{r}\,\sin(\omega t)}{z}|\psi_{i\sigma}(\mathbf{r},t)\rangle. \qquad (42)$$

The corresponding HHG power spectrum can now be obtained by the Fourier transformation of the respective time-dependent dipole moment or dipole acceleration:

$$P(\omega) = \left|\frac{1}{t_f-t_i}\int_{t_i}^{t_f} d(t)e^{-i\omega t}\,dt\right|^2 \equiv |d(\omega)|^2 \qquad (43)$$

and

$$P_A(\omega) = \left|\frac{1}{t_f-t_i}\frac{1}{\omega^2}\int_{t_i}^{t_f} d_A(t)e^{-i\omega t}\,dt\right|^2 \equiv |d_A(\omega)|^2. \qquad (44)$$

We note that an important measure of the accuracy of HHG results is that the power spectrum $P(\omega)$ should be equal to $P_A(\omega)$ if the time-dependent wave function calculation is fully converged.

1. The effect of dynamical electron correlation on the HHG of rare gas atoms

One recent application of the TDOEP/KLI-SIC formalism is to study the role of *dynamical electron correlation* on HHG of He atoms in intense linearly polarized (LP) laser pulses.[60] Of particular interest is the study of the mechanism responsible for the production of the "higher" harmonics observed in the experiment[74] which cannot be explained by the SAE model.[36,37] Figure 6 shows that while the SAE model fails to produce the higher harmonics, the TDDFT/KLI-SIC results agree well with the experimental data in both lower and higher HHG regimes, indicating the important role played by the dynamical electron correlation.[60] More detailed study of the HHG processes of rare gas (He, Ne, Ar) atoms has been recently reported.[75]

2. Coherent control of HHG of rare gas atoms in two-color mixed fields

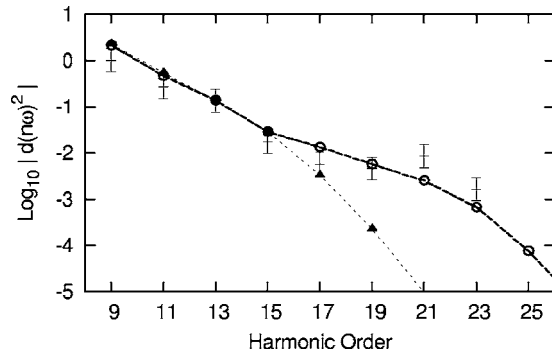The TDOEP/KLI-SIC formalism was recently extended to the study of coherent control of the production of HHG of

FIG. 6. The HHG spectrum of He obtained from the all-electron calculation (open circle) and from the SAE model (filled triangle). The experimental data (with error bar) are also shown for comparison. The HHG yields are normalized to the 13th harmonic peak. The laser peak intensity used in the calculation is $I = 3.5 \times 10^{15}$ W/cm^2 and wavelength $\lambda = 248.6$ nm.

He atoms by means of the use of two laser fields with different frequencies and polarization directions.[76] It is shown that by mixing a *weak* fundamental field (1053 nm) with a *strong* second-harmonic field (527 nm), one can produce high-order *sum* and *difference* frequency radiation and "even" harmonics with an efficiency similar to that of *odd* harmonics. Further the relative efficiency of the HHG can be controlled by manipulating the relative polarization direction of the two fields. These predictions are in accord with the recent experimental data.[77] As a case study, Fig. 7 shows the results (solid lines) of the HHG of He atoms in the mixed fields with the ω_o-field intensity $I_1 = 2 \times 10^{12}$ W/cm^2 and the $2\omega_o$-field intensity $I_2 = 4 \times 10^{14}$ W/cm^2. The fields are parallel to each other with the relative phase $\delta = 0$. Also shown in Fig. 7 for comparison are the single-field data, ω_o field alone (open circle) and $2\omega_o$ field alone (filled circle), both with laser intensity 4×10^{14} W/cm^2. First recall that the single-color $2\omega_o$ field produces $(4n+2)$ harmonics, $n = 0, 1, 2, \ldots$. By mixing the $2\omega_o$ field with a weak (200 times weaker) ω_o field, three additional $[(4n-1)$th, $4n$th, $(4n+1)$th] harmonics appear in between two adjacent harmonics of the single-$2\omega_o$ field case. The remarkable feature is that the intensities of these extra harmonics are of similar orders of magnitude of
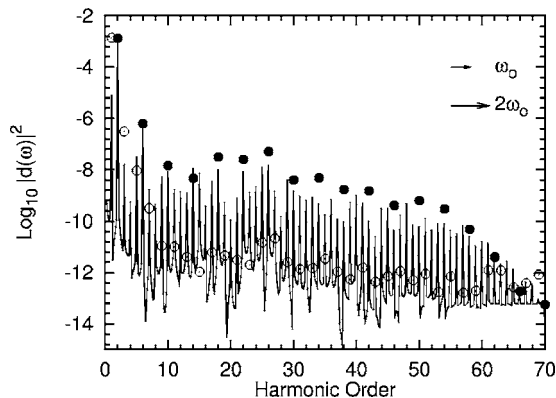
the harmonics produced by the single-color $2\omega_o$ field (filled circle) and are much higher than those produced by the single-color ω_o field (open circle). Further these $4n$th harmonics are the even harmonics which cannot be produced by either the single-color $2\omega_o$ or the single-color ω_o field alone. The generation of these extra harmonics can be explained by the high-order wave mixing mechanism. Thus the leading channel for producing the $(4n+1)$th harmonic is due to the absorption of $2n$ photons from the $2\omega_o$ field and one photon from the ω_o field. Similarly, the $(4n-1)$th harmonic is produced by the absorption of $2n$ photons from the $2\omega_o$ field and the emission of one photon to the ω_o field. Likewise, the even $(4n$th$)$ harmonics can be produced by the absorption of $(2n-1)$ photons from the $2\omega_o$ field and the absorption of two photons from the ω_o field. Thus the combination of a strong $2\omega_o$ field with a weak ω_o field can produce both odd and even harmonics with relatively high yields.[76]

3. Generation of circularly polarized HHG

In all the theoretical and experimental investigations up to 1998, only LP HHG has been studied. This is because the dipole selection rule excludes the possibility of producing *circularly polarized* (CP) harmonics by multiphoton mechanism. Recently a feasible scheme has been proposed for the generation of *purely* CP high harmonics, using two-color laser fields.[78] The proposed setup consists of a CP fundamental laser field ω and a LP second-harmonic laser field 2ω in *crossed-beam* configuration. The feasibility of such a scheme is confirmed by a three-dimensional TDOEP/KLI-SIC calculation of the He system.[78]

IV. SELF-INTERACTION-FREE TDDFT FOR MOLECULAR MULTIPHOTON PROCESSES IN INTENSE LASER FIELDS

A. TDDFT with OEP/KLI-SIC for molecular processes in intense laser fields

The TDOEP/KLI-SIC formalism described in the last section for atomic systems can be extended to the molecular systems. Consider the solution of the time-dependent Kohn–Sham-tpye (TDKS) equation for N-electron molecular systems (under fixed nuclei approximation) in LP laser fields, in atomic units,

$$i \frac{\partial}{\partial t} \psi_{i\sigma}(\mathbf{r}, t) = \hat{H}(\mathbf{r}, t) \psi_{i\sigma}(\mathbf{r}, t)$$

$$= \left[-\frac{1}{2} \nabla^2 + v_{\text{eff},\sigma}(\mathbf{r}, t) \right] \psi_{i\sigma}(\mathbf{r}, t),$$

$$i = 1, 2, \ldots, N_\sigma \qquad (45)$$

where $v_{\text{eff},\sigma}(\mathbf{r}, t)$ is the time-dependent effective potential depending upon the total electron density $\rho(t)$ and σ is the spin index. Following the TDOEP/KLI-SIC procedure, we obtain the time-dependent OEP as[60,79]

FIG. 7. HHG spectra of He atoms in the two-color mixed fields ($\omega_1 = \omega_o$, $\omega_2 = 2\omega_o$) with parallel polarization and laser intensities $I_1 = 2 \times 10^{12}$ W/cm^2, $I_2 = 4 \times 10^{14}$ W/cm^2 (solid line). Also shown are the results of HHG spectra in single-color ω_o (1053 nm) field (open circle) and single-color $2\omega_0$ (527 nm) field (filled circle), both with intensity at 4×10^{14} W/cm^2.

$$V_{\text{eff},\sigma}^{\text{OEP}}(\mathbf{r},t) = v_{\text{ext}}(\mathbf{r},t) + \frac{\delta J[\rho]}{\delta\rho_\sigma(\mathbf{r},t)} + V_{\text{SIC},\sigma}(\mathbf{r},t). \tag{46}$$

Here $v_{\text{ext}}(\mathbf{r},t)$ is the external potential due to the interaction of the electron with the external laser field and the nuclei and $V_{\text{SIC},\sigma}(\mathbf{r},t)$ is given in Eq. (35). For the special case of homonuclear diatomic molecules, the time-dependent OEP potential, Eq. (46), has the following explicit form:

$$V_{\text{eff},\sigma}^{\text{OEP}}(\mathbf{r},t) = -\frac{Z_1}{|\mathbf{R}_1 - \mathbf{r}|} - \frac{Z_2}{|\mathbf{R}_2 - \mathbf{r}|} + \int d^3r' \frac{\rho(\mathbf{r}',t)}{|\mathbf{r} - \mathbf{r}'|}$$
$$+ \mathbf{E}(t) \cdot \mathbf{r}\sin\omega t + V_{\text{SIC},\sigma}(\mathbf{r},t). \tag{47}$$

Here $\mathbf{r}$ is the electronic coordinate, $\mathbf{E}(t)$ the electric field amplitude, and $\mathbf{R}_1 = (0,0,a)$ and $\mathbf{R}_2 = (0,0,-a)$ are the coordinates of the two nuclei in Cartesian coordinates with nuclear charges Z_1 and Z_2, respectively. The internuclear separation R is equal to $2a$.

B. Generalized pseudospectral method for spatial discretization of two-center systems

In this section, we discuss a new procedure for the optimal spatial discretization and high-precision solution of field-free two-center (diatomic molecular) systems. We shall use the prolate spheroidal coordinates (μ,ν,φ), $0 < \mu < \infty$, $0 < \nu < \pi$, and $0 < \varphi < 2\pi$ for the description of the system:

$$x = a\sinh\mu\sin\nu\cos\varphi,$$

$$y = a\sinh\mu\sin\nu\sin\varphi,$$

$$z = a\cosh\mu\cos\nu.$$

Due to the axial symmetry of the diatomic systems, the field-free solution takes the form

$$\Psi_m(\mathbf{r}) = e^{im\varphi}\Phi(\mu,\nu), \quad m = 0, \pm 1, \pm 2, \ldots.$$

In order to symmetrize the Hamiltonian matrix, we transform the Kohn–Sham differential equation, Eq. (1), into a variational problem that minimizes the functional

$$F_s = \frac{1}{2}\int |\boldsymbol{\nabla}\psi|^2 d\mathbf{r} + \int (v_{\text{eff}} - \epsilon)|\psi|^2 d\mathbf{r}. \tag{48}$$

The Coulomb repulsive potential $V_c = \int d\mathbf{r}'[\rho(\mathbf{r}')/|\mathbf{r}-\mathbf{r}'|]$ satisfying the Poisson equation, $\nabla^2 V_c = -4\pi\rho$, can also be recast into the following variational form seeking the minimization of

$$F_c = \frac{1}{2}\int |\boldsymbol{\nabla}V_c|^2 d\mathbf{r} - 4\pi\int \rho V_c d\mathbf{r}. \tag{49}$$

The GPS technique for one-center (atomic) system[49,50] can be extended to *discretize* the integral representation in two-center systems.[79,80] In the two-center GPS procedure, one expands any spatial wave function $\Phi(\mu,\nu)$ by $\Phi_{N_\mu,N_\nu}(\mu,\nu)$, the polynomials of order N_μ and N_ν in μ and ν, respectively,
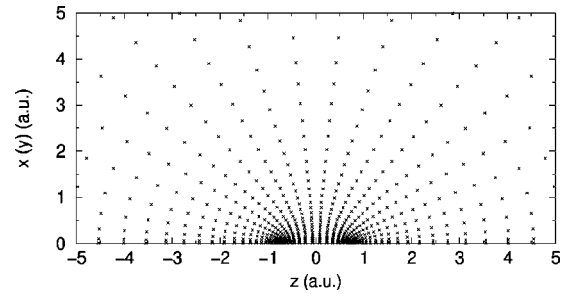

FIG. 8. The grid structure of the spatial coordinates of H_2 obtained by the generalized pseudospectral discretization technique.

$$\Phi(\mu,\nu) \simeq \Phi_{N_\mu,N_\nu}(\mu,\nu) = \sum_{i=0,j=0}^{N_\mu,N_\nu} \phi(\mu_i,\nu_j)g_i[x(\mu)]g_j[y(\nu)], \tag{50}$$

and further require the approximation to be exact at the collocation points, i.e., $\Phi_{N_\mu,N_\nu}(\mu_i,\nu_j) = \phi(\mu_i,\nu_j) \equiv \phi_{ij}$, where $\{x(\mu_i)\}$ and $\{y(\nu_j)\}$ are the two sets of collocation points to be described below. In Eq. (50), $g_i(x)$ and $g_j(y)$ are the cardinal functions[49,50,81] defined as

$$g_i(x) = -\frac{1}{N_\mu(N_\mu+1)P_{N_\mu}(x_i)}\frac{(1-x^2)P'_{N_\mu}(x)}{x-x_i}, \tag{51}$$

$$g_j(y) = -\frac{1}{N_\nu(N_\nu+1)P_{N_\nu}(y_j)}\frac{(1-y^2)P'_{N_\nu}(y)}{y-y_j}. \tag{52}$$

In the case of the Legendre pseudospectral method,[49,79–81] the collocation points are determined, respectively, by the roots of the first derivative of the Legendre polynomial P_{N_μ} with respect to x and the first derivative of P_{N_ν} with respect to y, namely,

$$P'_{N_\mu}(x_i) = 0, \quad P'_{N_\nu}(y_j) = 0. \tag{53}$$

It follows that the cardinal functions possess the following unique and desirable properties

$$g_i(x_{i'}) = \delta_{i,i'}, \quad g_j(y_{j'}) = \delta_{j,j'}. \tag{54}$$

The mapping relationships between μ and x and between ν and y can be chosen as[79,80]

$$\mu = L\frac{1+x}{1-x}, \quad \nu = \frac{\pi}{2}(1+y), \tag{55}$$

where $x \in [-1,1]$, $y \in [-1,1]$, $\mu \in [0,\infty]$, $\nu \in [0,\pi]$, and L is a mapping parameter.

A more detailed discussion of the construction of the differentiation matrix and the symmetrization of the Hamiltonian matrix can be found elsewhere.[79,80] A major advantage of the outlined generalized pseudospectral method is that it allows for *nonuniform* optimal spatial grid discretization: *denser* mesh near the nuclei and *sparser* mesh for long-range part of the Coulombic potential. With the use of only a modest number of grid points, high precision eigenvalues and eigenfunctions can be obtained. Figure 8 shows a typical grid structure for two-center diatomic systems.[79,80] As a measure of the accuracy of the GPS procedure, we have first tested

the method for the H_2^+ molecule, where exact results are available for comparison. Using only a modest number of grid points (20 for the μ coordinate and 9 for the ν coordinate), we obtain the ground-state energy to be $-1.102\ 634\ 214\ 494\ 9$ a.u., in complete agreement with the exact value of $-1.102\ 634\ 214\ 494\ 9$ a.u.[82]

C. Time-dependent generalized pseudospectral method for numerical solution of self-interaction-free TDDFT equations in two-center systems

In the following, we extend the TDGPS procedure to the numerical solution of the time-dependent OEP/SIC equations in two-center systems. Consider the solution of time-dependent Kohn–Sham-type equation with OEP/SIC for N-electron diatomic molecular systems in LP laser fields,

$$i\frac{\partial}{\partial t}\psi_{i\sigma}(\mathbf{r},t) = \hat{H}\psi_{i\sigma}(\mathbf{r},t) = [\hat{H}_0(\mathbf{r}) + \hat{V}(\mathbf{r},t)]\psi_{i\sigma}(\mathbf{r},t),$$

$$i = 1,2,\ldots,N_\sigma. \tag{56}$$

Here $\hat{H}_0$ is the time-independent Hamiltonian with OEP/SIC at $t=0$ and $\hat{V}$ includes the electron-laser field interaction and the residual time-dependent OEP/SIC:

$$\hat{H}_0(\mathbf{r}) = -\frac{1}{2a^2}\left\{ \frac{1}{(\sinh^2\mu + \sin^2\nu)\sinh\mu}\frac{\partial}{\partial\mu}\left(\sinh\mu\frac{\partial}{\partial\mu}\right) \right.$$
$$\left. + \frac{1}{(\sinh^2\mu + \sin^2\nu)\sin\nu}\frac{\partial}{\partial\nu}\left(\sin\nu\frac{\partial}{\partial\nu}\right)\right\}$$
$$+ V_{\mathrm{SIC},\sigma}^{\mathrm{OEP}}(\mathbf{r},0), \tag{57}$$

$$\hat{V}(\mathbf{r},t) = -\mathbf{E}(t)\cdot\mathbf{r}\sin\omega t + V_{\mathrm{SIC},\sigma}^{\mathrm{OEP}}(\mathbf{r},t) - V_{\mathrm{SIC},\sigma}^{\mathrm{OEP}}(\mathbf{r},0), \tag{58}$$

where $\mathbf{E}(t)$ is the electric field, assumed to be parallel to the internuclear ($\hat{z}$) axis, and $E(t)=Ff(t)$, where $f(t)$ is the envelope function of the laser pulse. The second- (or higher) order split-operator technique in prolate spheroidal coordinates and in the *energy* representation can be extended for accurate and efficient propagation of the time-dependent OEP/SIC equations:[66,79,80]

$$\psi_{i\sigma}(\mathbf{r},t+\Delta t) \simeq e^{-i\hat{V}(\mathbf{r},t)\Delta t/2}e^{-i\hat{H}_0(\mathbf{r})\Delta t}$$
$$\times e^{-i\hat{V}(\mathbf{r},t)\Delta t/2}\psi_{i\sigma}(\mathbf{r},t) + O(\Delta t^3). \tag{59}$$

Note that such an expression is different from the conventional split-operator techniques,[62,63,83] where $\hat{H}_0$ is usually chosen to be the kinetic energy operator and $\hat{V}$ the remaining Hamiltonian depending on the spatial coordinates only. The use of the energy representation in Eq. (59) allows the explicit *elimination* of the undesirable fast-oscillating *high-energy* components and speeds up considerably the time propagation.[66,79,80] In addition, the symmetry properties possessed by $\hat{H}_0$ can be used to simplify and facilitate the calculations.
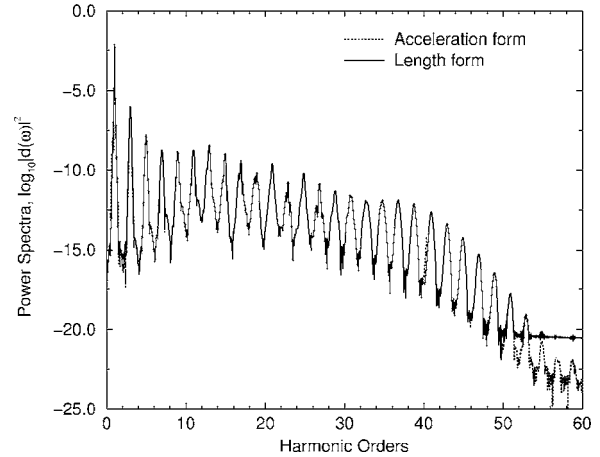

FIG. 9. The HHG power spectrum of H_2 (at $R=1.4a_0$) in a 20 optical cycle, 1064 nm, $\sin^2$ pulse shape laser fields with peak intensity 10^{14} W/cm^2. Both the length form (solid line) and acceleration form (dotted line) power spectra are shown for comparison.

D. Exploration of the underlying mechanisms for high harmonic generation H_2 in intense laser fields

In this section we show an application of the TDOEP/KLI-SIC procedure to the study of HHG of H_2 in intense pulsed laser fields. First we discuss the field-free electronic structure calculations using the steady-state OEP/KLI-SIC procedure,[21,79] and the GPS procedure[79,80] is extended to discretize the molecular Hamiltonian in the prolate spheroidal coordinates. For H_2, the calculated ground-state energy is -1.1336 a.u. (using LSDA exchange energy functional only) and -1.1828 a.u. (including both LSDA exchange and correlation energy functionals); the latter is within 1% of the exact value of $-1.174\ 448$ a.u. If the GGA energy functional such as that of BLYP (Ref. 1) is used, the calculated ground-state energy is improved to $-1.174\ 44$ a.u.

Consider now the interaction of H_2 molecules with an intense LP laser field with wavelength 1064 nm, $\sin^2$ pulse shape, and 20 optical cycles in pulse length. The time-dependent xc potential is constructed by means of the time-dependent OEP/KLI-SIC procedure using the adiabatic LSDA exchange and correlation energy functional. We shall assume the electric field polarization is aligned along the internuclear-axis ($\hat{z}$) direction. This approximation is justified by the experimental observation that the laser-molecular interaction tends to force the molecule to align along the polarization axis. In the following, we shall focus our discussion on the HHG process of H_2 molecules from the ground vibrational state with the internuclear separation R fixed at the equilibrium distance ($R=R_e=1.4a_0$). The fixed nuclei approximation is justifiable since the zero-point vibration of H_2 in the ground state is rather small (within $0.25a_0$ of R_e) and the inclusion of the vibrational degree of freedom is not expected to alter the main features of the HHG phenomenon, particularly when the time duration of the laser pulse is short.

The solution of the TDOEP/KLI-SIC equation is performed by means of the TDGPS method described above. As an example of the numerical accuracy of the TDGPS technique, Fig. 9 shows the comparison of the HHG power spectrum of H_2 for the case of laser intensity $I=10^{14}$ W/cm^2
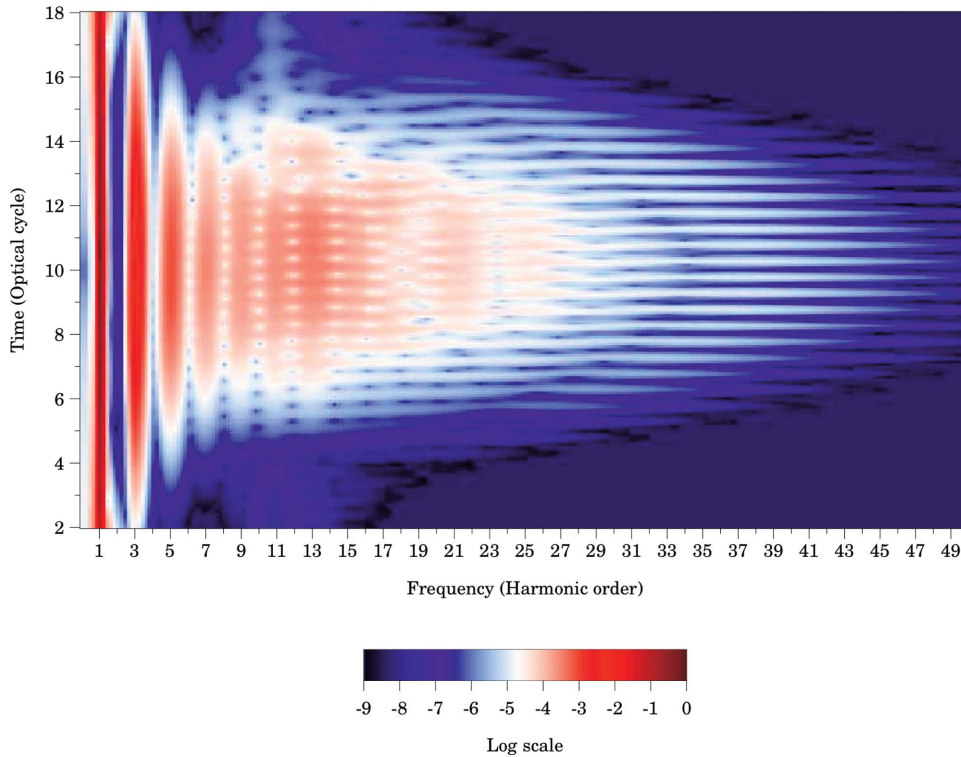
FIG. 10. (Color). The time-frequency spectra (modulus) of H_2 (at $R=1.4a_0$) in (1064 nm, 20 optical cycle, $\sin^2$ pulse shape) laser fields with peak intensity 10^{14} W/cm^2. The colors shown are in logarithmic scale (in the powers of 10).

obtained by the Fourier transform of the induced dipole and dipole acceleration, respectively. Excellent agreement of the two spectra is obtained from the lowest harmonics all the way to the cutoff regime, indicating the the full convergence of the time-dependent wave functions.

Figure 9 shows that those harmonic peaks near the cutoff regime are structureless. However, for harmonics in the plateau and well below the cutoff, they possess some multiple-peak fine structures. To explore the detailed spectral and temporal structure of HHG and the underlying mechanisms in different energy regimes, one can perform the time-frequency analysis by means of the wavelet transform[84,85] of the induced dipole (or dipole acceleration),

$$A_W(t_0, \omega) = \int d(t) W_{t_0, \omega}(t) dt \equiv d_\omega(t), \tag{60}$$

with the wavelet kernel $W_{t_0, \omega}(t) = \sqrt{\omega} W[\omega(t-t_0)]$. For the harmonic emission, a natural choice of the mother wavelet is given by the Morlet wavelet[85]

$$W(x) = (1/\sqrt{\tau}) e^{ix} e^{-x^2/2\tau^2}. \tag{61}$$

Figure 10 shows the modulus of the time-frequency profiles of H_2 (at $R=1.4a_0$) in (1064 nm, 20 optical cycle, $\sin^2$ pulse shape, and 10^{14} W/cm^2) laser fields, revealing striking and vivid details of the spectral and temporal structures. Several salient features are noticed. First, for the lowest few harmonics, the time profile (at a given frequency) shows a smooth function of the driving laser pulse. This is an indication that the *multiphoton* mechanism dominates this lower harmonic regime. In this regime, the probability of absorbing N photons is roughly proportional to I^N, and I (laser intensity) is proportional to $E(t)^2$. Second, the smooth time profile is getting shorter (in time duration) and broadened (in fre-

quency) as the harmonic order is increased, as is evident in Fig. 10 from the first to the seventh harmonics. As the harmonic order is further increased, the time profiles (see particularly the 11th harmonic in Fig. 10) develop extended fine structures. This can be attributed to the effect of excited states and the onset of the ionization threshold. Third, for those high harmonics in the plateau regime well above the ionization threshold, the most prominent feature is the development of fast burst time profiles. At a given time, we see that such bursts actually form a *continuous frequency profile* in Fig. 10. This is clear evidence of the existence of the bremsstrahlung radiation emitted by each recollision of the electron wave packet with the parent ionic core(s). In contrast, we find that the (multiphoton-dominant) lowest-order harmonics form a *continuous time profile* at a given frequency. In the intermediate energy regime where both multiphoton and tunneling mechanisms contribute, the time-frequency profiles show a netlike structure. More detailed analysis of the origin of the power spectrum patterns near and below the cutoff can be pursued by performing the cross section of the time-frequency profile of Fig. 10 at a given harmonic frequency.[79]

Finally it will be instructive to explore the origin of the fine-structure peak splitting of harmonics in the plateau regime below the cutoff, see for example, the 23rd harmonic in Fig. 9. Figure 11 shows the time profiles at the three subpeak positions (denoted by 1, 2, and 3) within the 23rd harmonic. Strikingly, their time profiles nearly coincide. This is evidence that all the harmonic subpeaks within a given harmonic are produced by the same mechanism, namely, they are produced by the interference in time of all the bremsstrahlung radiation emitted from all the returning electronic wavepackets within the incident laser pulse duration. To our knowledge, this is the first *ab initio* calculation exhibiting the
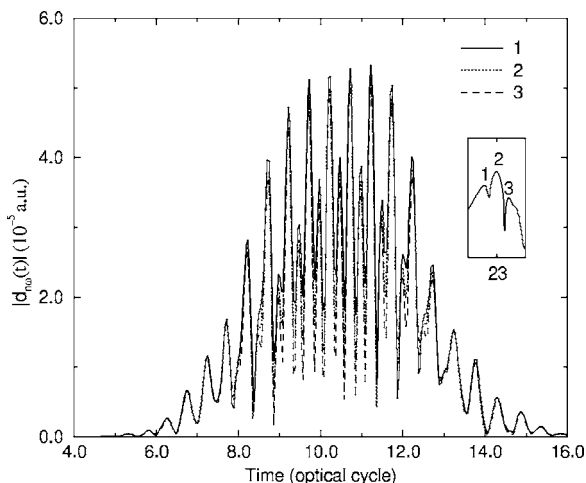
FIG. 11. The time profiles of the subpeaks of the 23rd harmonic of H_2 ($R=1.4a_0$) in intense pulsed laser fields. The laser parameters are the same as those in Fig. 3.

details of the time profiles of the subpeak harmonics for a molecular system.

E. Multiphoton ionization and high harmonic generation of N₂ in intense laser fields

In the last section, we describe the TDOEP/KLI-SIC method for the study of multiphoton processes of molecular systems in intense laser fields, taking into account the correct long-range Coulombic ($-1/r$) potential. Here we consider an alternative and simpler procedure by adopting the improved Leeuwen–Baerends (LB)α type potential,[86] $v_{xc\sigma}^{LB\alpha}$, for the static xc potential. The corresponding time-dependent xc potential in the adiabatic approximation consists of two empirical parameters α and β and possesses the following explicit form,[87]

$$v_{xc\sigma}^{LB\alpha}(\mathbf{r},t) = \alpha v_{x\sigma}^{LSDA}(\mathbf{r},t) + v_{c\sigma}^{LSDA}(\mathbf{r},t)$$
$$- \frac{\beta x_\sigma^2(\mathbf{r},t)\rho_\sigma^{1/3}(\mathbf{r},t)}{1 + 3\beta x_\sigma(\mathbf{r},t)\ln\{x_\sigma(\mathbf{r},t) + [x_\sigma^2(\mathbf{r},t)+1]^{1/2}\}}. \tag{62}$$

The first two terms in Eq. (62), $v_{x\sigma}^{LSDA}$ and $v_{c\sigma}^{LSDA}$ are the LSDA exchange and correlation potentials which do *not* have the correct asymptotic behavior. The last term in Eq. (62) is the nonlocal gradient correction with $x_\sigma(\mathbf{r}) = |\nabla\rho_\sigma(\mathbf{r})|\rho_\sigma(\mathbf{r})^{4/3}$, which ensures the proper long-range asymptotic behavior $v_{xc\sigma}^{LB\alpha} \rightarrow -1/r$ as $r \rightarrow \infty$. For the time-independent case, this exchange-correlation LBα potential has been found to be reliable for the electronic structure and frequency-dependent (hyper) polarizability calculations of a number of atomic and molecular systems.[86]

Figure 12 presents an example of the time-dependent single-electron populations of different spin orbitals of N_2 molecule.[87] The slope of the decay of the electron population in time describes the ionization rate. The laser (electric) field (with intensity 10^{14} W/cm^2 and wavelength 1064 nm) is assumed to be parallel to the internuclear axis and the internuclear distance of N_2 is fixed at its equilibrium position, $R_e = 2.072a_0$. In this case, the order of ionization probability is
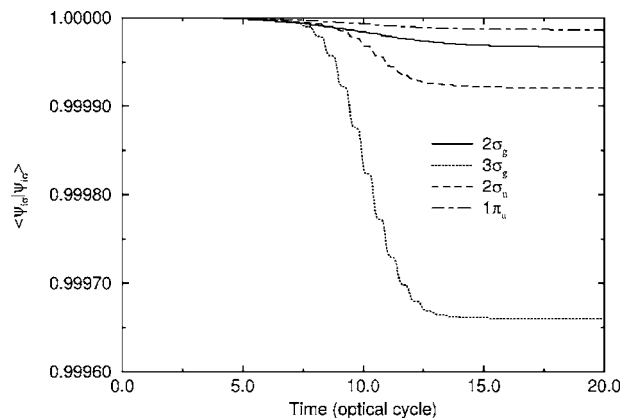

FIG. 12. The time-dependent population of electrons in different spin orbitals of N_2 in 10^{14} W/cm^2, 1064 nm, $\sin^2$ pulse laser field with 20 optical cycles in pulse duration.

found to be $1\pi_u < 2\sigma_g < 2\sigma_u < 3\sigma_g$. On the other hand, for the 3×10^{14} W/cm^2 and 1064 nm pulses (not shown), the order of ionization probability is $2\sigma_g < 1\pi_u < 2\sigma_u < 3\sigma_g$. Thus within the σ electrons, the lower the electron orbital binding energy (ionization potential) is, the more will be the electron ionization probability. However, although the ionization potential of $1\pi_u$ electrons is lower than that of $2\sigma_u$ electrons, the ionization probability of $1\pi_u$ electrons turns out to be less than that of $2\sigma_u$ electrons in all the cases. This can be attributed to the fact that $2\sigma_u$ orbital is along the electric field direction $\hat{E}$, while that of $1\pi_u$ is perpendicular to $\hat{E}$. We thus see two different effects that can contribute to the ionization: the ionization potential (electron binding energy) effect and the orbital orientation effect. The ionization potential effect makes the electrons with lower ionization potentials easier to ionize. The orientation effect makes the ionization easier for those electrons whose orbital orientations are parallel to the electric field. These two effects are clearly competing.

We now discuss briefly the results of the *all-electron* HHG calculations of N_2.[87] The relative contribution of individual spin orbital to HHG, $d_{i\sigma}(\omega)$, depends on the harmonic frequency range but in general it follows roughly the same trend as the order of time-dependent induced dipole moment.[87] The total HHG power spectrum is obtained by the sum of individual spin-orbital HHG power spectrum $d_{i\sigma}(\omega)$ plus the interference terms. For the case of N_2, we observe interesting constructive and destructive interferences between the two highest occupied bond $3\sigma_g$ and anti-bonding $2\sigma_u$ orbitals: It is the interference between these two largest induced dipoles ($d_{3\sigma_g}$ and $d_{2\sigma_u}$) that contributes dominantly to the overall HHG power spectrum of N_2.[87] Thus for many-electron molecular systems such as N_2, the conventional *single-active-electron* (SAE) model is not valid, since there is no single electron molecular orbital which dominates the total HHG process.

V. GENERALIZED FLOQUET FORMULATION OF TIME-DEPENDENT DENSITY-FUNCTIONAL THEORY IN PERIODIC OR QUASIPERIODIC FIELDS

In the last few sections, the time-dependent equations in the self-interaction-free TDDFT formulations are solved nu-

merically by propagating individual spin-orbital wave function in time in a self-consistent fashion. We call this procedure the *time-dependent* approach to TDDFT. It is a natural approach for problems involving *short pulsed* laser fields where the atom (molecule)-field interaction Hamiltonian can be an arbitrary function of time. There is, however, other important class of problems that the Hamiltonian is either a *periodic* function of time (such as the cases involving continuous wave, monochromatic, or *long* pulse laser fields) or a *quasiperiodic* (nonperiodic) function of time (such as the cases of polychromatic or multicolor fields where the light frequencies are incommensurate). In this case, it is advantageous to employ the *generalized Floquet theories*[88–91] which allow the exact transformation of the periodic or quasiperiodic time-dependent Schrödinger equation into an equivalent time-independent Floquet matrix eigenvalue problem. The time-independent Floquet formulation and its various generalized formalisms[88–91] developed in the last two decades have been extensively used for the nonperturbative treatment of numerous atomic and molecular multiphoton and nonlinear optical processes in intense one-color and multicolor laser fields. The time-independent Floquet approaches, when they are applicable, have several advantages over the time-dependent approaches. First, the Floquet approach is numerically more accurate since it involves only the solution of a (Hermitian or non-Hermitian) time-independent Floquet matrix eigenvalue problem and does not suffer the time-propagation errors as in the time-dependent methods. Second, the *Floquet-state* or *dressed-state* picture provides useful physical insights regarding the multiphoton dynamics in terms of the *avoided crossing* pattern of involved *quasienergy levels*. Third, for *near-resonant* multiphoton processes, the *nearly degenerate* (high-order) perturbation theory can be applied to the Floquet Hamiltonian, allowing the reduction of the infinite dimensional Floquet matrix into a $N \times N$ effective Hamiltonian (where N is the number of atomic or molecular states considered). This leads to *analytical* expressions and insights valuable for both theoretical and experimental investigation of multiphoton and very high-order nonlinear optical phenomena.[89]

The recent development of the generalized Floquet formulation of TDDFT allows the combination of Floquet approach with TDDFT and opens up a powerful new nonperturbative time-independent theoretical framework for the study of multiphoton and nonlinear optical processes of many-electron quantum systems (atoms, molecules, solids, condensed matter, etc.) in intense laser fields.[92–96] In the Floquet formulation of TDDFT,[92] it is shown that the time-dependent) Kohn–Sham equation in periodic fields can be exactly transformed into an equivalent time-independent Floquet matrix eigenproblem whose eigenvalues (*quasienergies*) are *unique* functionals of the electron spin density. Further for the bound-free transitions, the notions of "complex" density, complex equation of continuity, and non-Hermitian Floquet formalism can be introduced to facilitate the study of multiphoton ionization (dissociation) processes.[92] Initial application to the study of multiphoton ionization of He atoms[92] yields results in good agreement of the experimental data. More recent extensions of the generalized Floquet-

TDDFT formalism include the *many-mode* Floquet formulation of the multicolor or quasiperiodic laser excitation case,[93] Floquet formulation of time-dependent *current* density functional theory[94] (TDCDFT), and exterior-complex-scaling-generaiized-pseudospectral technique[95] for the calculation of the complex quasienergies of many-electron quantum systems.

Extension of the Floquet-TDDFT formalisms to the study of multiphoton processes of atoms,[93] negative ions,[95] and molecules such as above-threshold multiphoton ionization, molecular multiphoton dissociation, HHG, and high-order nonlinear optical susceptibilities, etc., is in progress and will be reported elsewhere.

VI. PERSPECTIVES

In this paper, we have surveyed several self-interaction-free DFT and TDDFT approaches recently developed for more accurate treatment of the electronic structure and time-dependent dynamics of many-electron quantum systems. They allow the construction of orbital-independent single-particle local potential which is self-interaction free and possesses the correct long-range asymptotic Coulombic ($-1/r$) potential behavior. Using such procedures, the autoionizing resonances and excited states can now be treated more adquately and the energy of the highest occupied spin orbital provides a good approximation to the ionization potential.[21] The generalized pseudospectral (GPS) technique allows the construction of nonuniform and optimal spatial grids, denser mesh near to each nucleus and sparser mesh at longer range, leading to high-precision solution of both electronic structure and time-dependent quantum dynamics with the use of only a modest number of spatial grid points. The TDDFT/OEP-SIC formalism along with the use of the time-dependent GPS numerical technique allows nonperturbative in-depth exploration of strong field processes, such as the study of the underlying physical mechanisms of the multiple high-order harmonic generation (HHG) phenomenon, at an unprecedented detail.

At this time, the TDDFT is the primary approach available for the treatment of time-dependent processes of many-electron quantum systems in strong fields. Further extension of the self-interaction-free TDDFT approaches to larger molecular systems will be valuable and can lead to significant advancement in the understanding of strong-field chemical physics and atomic and molecular physics in the future.

The alternative approach, the Floquet formulation of TDDFT and TDCDFT, provides a complementary and powerful time-independent framework for nonperturbative treatment of many-electron quantum systems in periodic or quasiperiodic time-dependent fields. One important future direction is the extension of the Floquet-TDDFT formulation to the *ab initio* investigation of high-order nonlinear optical processes of complex systems. More development is required for accurate treatment of molecular systems.

We note that another alternative approach, the quantum fluid dynamics (QFD) approach of DFT (Refs. 59 and 97), seems to also be promising. A unique feature of the combined QFD and DFT approach is that a single generalized

nonlinear Schrödinger-type equation can be derived.[98] Further, the QFD formulation is conceptually appealing, since the electron cloud can be treated as a "classical fluid" moving under the influence of classical Coulomb forces and an additional quantum potential. The QFD-TDDFT approach has been recently shown to be capable of providing good description of strong-field processes of rare gas atoms, provided that the QFD nonlinear equations can be solved accurately.[99,100] Future extension of the QFD-TDDFT approach to larger systems, such as clusters, will be particularly interesting and may lead to instructive fluid dynamics picture and useful physical insights for the understanding of the quantum dynamic behavior of many-particle systems.

Finally we would like to point out some of the open questions that remain to be answered by future more comprehensive treatment. First, as mentioned in the TDDFT sections, most of the strong-field calculations so far have used the adiabatic approximation. Although such an approximation is likely to be adequate for weak and intermediate field strengths, its validity in very strong fields remains to be investigated. However, as pointed out in Eqs. (30) and (33), those memory-effect terms beyond the adiabatic approximation are actually identical to zero, if the conventional xc-energy functional (such as that in LSDA and GGA) is adopted. This may partially account for the success of recent strong-field studies. Like the steady-state case, the exact form of time-dependent (TD) xc-energy functional is unknown. More rigorous nonadiabatic treatment of the TD xc-energy functional can be facilitated if some information regarding the TD electron density for N-electron systems can be determined by means of the *ab initio* wave-function approach. But this task is not feasible at the current time for $N > 2$. Note that the exact TD xc-energy functional form is supposed to be universal and independent of N. Thus the information of the strong-field behavior of the simplest but nontrivial two-electron systems will be very valuable for the future construction of TD xc-energy functional. Another direction to improve the TD xc-energy functional is to establish some exact relationships that must be satisfied by an exact TD xc-energy functional.[96,101–103] Such exact relations do not actually provide any suggested energy functional form but they can serve as useful constraints for the future search of more accurate TD xc-energy functional.

Another open question is regarding the feasibility of the current TDDFT approaches for the treatment of multiple electron ionization processes. Several recent treatments of the nonsequential and double ionization processes of rare gas atoms in strong fields show that the current TDDFT methodology seems to be not yet mature enough to provide satisfactory results. More investigation in this direction will be needed in the future.

ACKNOWLEDGMENTS

[1] R. G. Parr and W. T. Yang, *Density-Function Theory of Atoms and Molecules* (Oxford University Press, New York, 1989).
[2] *Density Functional Methods in Chemistry*, edited by J. K. Labanowski and J. W. Andzelm (Springer, Berlin, 1991).
[3] N. H. March, *Electron Density Theory of Atoms and Molecules* (Academic, San Diego, 1992).
[4] *Density Functional Theory*, NATO ASI, Ser. B., edited by E. K. U. Gross and R. M. Dreizler (Plenum, New York, 1995), Vol. 337.
[5] E. K. U. Gross, F. J. Dobson, and M. Petersilka, *Density Functional Theory* (Springer, New York, 1996), p. 81.
[6] *Electronic Density Functional Theory: Recent Progress and New Directions*, edited by J. Dobson, G. Vignale, and M. P. Das (Plenum, New York, 1997).
[7] P. Hohenberg and W. Kohn, Phys. Rev. **136**, B864 (1964).
[8] W. Kohn and L. J. Sham, Phys. Rev. **140**, A1133 (1965).
[9] A. Görling, Phys. Rev. A **54**, 3912 (1996).
[10] R. Singh and B. M. Deb, Phys. Rep. **311**, 47 (1999).
[11] M. Lévy and Á. Nagy, Phys. Rev. Lett. **83**, 4361 (1999).
[12] V. N. Glushkov and A. K. Theophilou, Phys. Rev. A **64**, 064501 (2001).
[13] M. K. Harbola, Phys. Rev. A **65**, 052504 (2002).
[14] A. K. Roy and S. I. Chu, Phys. Rev. A **65**, 052508 (2002).
[15] M. Slamet, R. Singh, L. Massa, and V. Sahni, Phys. Rev. A **68**, 042504 (2003).
[16] S. J. Vosko, L. Wilk, and M. Nusair, Can. J. Phys. **58**, 1200 (1980).
[17] C. Lee, W. Yang, and R. G. Parr, Phys. Rev. B **37**, 785 (1988).
[18] A. D. Becke, Phys. Rev. A **38**, 3098 (1988).
[19] J. P. Perdew and Y. Wang, Phys. Rev. B **33**, 8800 (1986).
[20] Q. Zhao and R. G. Parr, Phys. Rev. A **46**, R5320 (1992).
[21] X. M. Tong and S. I. Chu, Phys. Rev. A **55**, 3406 (1997).
[22] J. P. Perdew and A. Zunger, Phys. Rev. B **23**, 5048 (1981).
[23] E. Runge and E. K. U. Gross, Phys. Rev. Lett. **52**, 997 (1984).
[24] E. K. U. Gross and W. Kohn, Phys. Rev. Lett. **55**, 2850 (1985).
[25] A. Zangwill and P. Soven, Phys. Rev. A **21**, 1561 (1980).
[26] G. D. Mahan and K. R. Subbaswamy, *Local Density Theory of Polarizability* (Plenum, New York, 1990).
[27] M. Petersilka, U. J. Gossmann, and E. K. U. Gross, Phys. Rev. Lett. **76**, 1212 (1996).
[28] M. E. Casida, in *Recent Advances in Density-Functional Methods*, edited by D. P. Chong (World Scientific, Singapore, 1995), p. 155.
[29] M. E. Casida, in *Recent Developments and Applications of Modern Density Functional Theory*, edited by J. M. Seminario (Elsevier, Amsterdam, 1996).
[30] C. P. Hsu, S. Hirata, and M. Head-Gordon, J. Phys. Chem. A **105**, 451 (2001).
[31] G. Onida, L. Reining, and A. Rubio, Rev. Mod. Phys. **74**, 601 (2002).
[32] V. P. Osinga, S. J. A. van Gisbergen, J. G. Snijders, and E. J. Baerends, J. Chem. Phys. **106**, 5091 (1997).
[33] U. Hohm, D. Goebel, and S. Grimme, Chem. Phys. Lett. **272**, 1059 (1997).
[34] K. Yabana and G. F. Bertsch, Phys. Rev. A **60**, 1271 (1999).
[35] J. R. Chelikowsky, L. Kronik, and I. Vasiliev, J. Phys.: Condens. Matter **15**, R1517 (2003).
[36] A. L'Huillier, K. J. Schafer, and K. C. Kulander, J. Phys. B **24**, 3315 (1991).
[37] J. L. Krause, K. J. Schafer, and K. C. Kulander, Phys. Rev. A **45**, 4998 (1992).
[38] R. T. Sharp and G. K. Horton, Phys. Rev. **90**, 317 (1953).
[39] J. D. Talman and W. F. Shadwick, Phys. Rev. A **14**, 36 (1976).
[40] J. Krieger, Y. Li, and G. Iafrate, Phys. Lett. A **146**, 256 (1990); Phys. Rev. A **45**, 101 (1992); **46**, 5453 (1992).
[41] M. Norman and D. Koelling, Phys. Rev. B **30**, 5530 (1984).
[42] J. Perdew, R. Parr, M. Levy, and J. J. L. Balduz, Phys. Rev. Lett. **49**, 1691 (1982).
[43] K. Codling, R. P. Madden, and D. L. Ederer, Phys. Rev. **155**, 26 (1967).
[44] P. G. Burke and K. T. Taylor, J. Phys. B **8**, 2620 (1975).
[45] A. K. Rajagopal and J. Callaway, Phys. Rev. B **7**, 1912 (1973).
[46] A. H. MacDonald and S. H. Vosko, J. Phys. C **12**, 2977 (1979).

[47] M. V. Ramana and A. K. Rajagopal, Adv. Chem. Phys. **54**, 231 (1983).

[48] X. M. Tong and S. I. Chu, Phys. Rev. A **57**, 855 (1998).

[49] G. Yao and S. I. Chu, Chem. Phys. Lett. **204**, 381 (1993).

[50] J. Wang, S. I. Chu, and C. Laughlin, Phys. Rev. A **50**, 3208 (1994).

[51] M. Kastner, Phys. Today **46**(1), 24 (1993).

[52] L. Jacak, P. Hawrylak, and A. Wojs, *Quantum Dots* (Springer, New York, 1989).

[53] S. Tarucha, D. G. Austing, T. Honda, R. J. van der Hage, and L. P. Kouwenhoven, Phys. Rev. Lett. **77**, 3613 (1996).

[54] N. Fujito, A. Natori, and H. Yasunaga, Phys. Rev. B **53**, 9952 (1996).

[55] M. Macucci, K. Hess, and G. J. Iafrate, Phys. Rev. B **55**, R4879 (1997).

[56] I. H. Lee, V. Rao, R. M. Martin, and J.-P. Leburton, Phys. Rev. B **57**, 9035 (1998).

[57] T. F. Jiang, X. M. Tong, and S. I. Chu, Phys. Rev. B **63**, 045317 (2001).

[58] F. Bloch, Z. Phys. **81**, 363 (1933).

[59] B. M. Deb and S. K. Ghosh, J. Chem. Phys. **77**, 342 (1982).

[60] X. M. Tong and S. I. Chu, Phys. Rev. A **57**, 452 (1998).

[61] C. A. Ullrich, U. J. Grossmann, and E. K. U. Gross, Phys. Rev. Lett. **74**, 872 (1995).

[62] M. R. Hermann and J. A. Fleck, Jr., Phys. Rev. A **38**, 6000 (1988).

[63] T. F. Jiang and S. I. Chu, Phys. Rev. A **46**, 7322 (1992).

[64] K. C. Kulander, Phys. Rev. A **36**, 2726 (1987).

[65] C. A. Ullrich and E. K. U. Gross, Comments At. Mol. Phys. **33**, 211 (1997).

[66] X. M. Tong and S. I. Chu, Chem. Phys. **217**, 119 (1997).

[67] M. D. Perry and G. Mourou, Science **264**, 917 (1991).

[68] J. Zhou, J. Peatross, M. M. Murnane, H. C. Kapteyn, and I. P. Christov, Phys. Rev. Lett. **76**, 752 (1996).

[69] I. P. Christov, J. Zhou, J. Peatross, A. Rundquist, M. M. Murnane, and H. C. Kapteyn, Phys. Rev. Lett. **77**, 1743 (1996).

[70] C. Kan, N. H. Burnett, C. E. Capjack, and R. Rankin, Phys. Rev. Lett. **79**, 2971 (1997).

[71] Z. Chang, A. Rundquist, H. Wang, M. M. Murnane, and H. C. Kapteyn, Phys. Rev. Lett. **79**, 2967 (1997).

[72] M. Schnürer, Ch. Spielmann, P. Wobrauschek *et al.*, Phys. Rev. Lett. **80**, 3236 (1998).

[73] For a review, see A. L'Huillier, L. A. Lompre, G. Mainfray, and C. Manus, *Advances in Atomic, Molecular and Optical Physics*, Suppl. 1, edited by M. de Gravila (Academic, New York, 1992), p. 139.

[74] N. Sarukura, K. Hata, T. Adachi, R. Nodomi, M. Watanabe, and S. Watanabe, Phys. Rev. A **43**, 1669 (1991).

[75] X. M. Tong and S. I. Chu, Phys. Rev. A **64**, 013417 (2001).

[76] X. M. Tong and S. I. Chu, Int. J. Quantum Chem. **69**, 293 (1998).

[77] M. D. Perry and J. K. Crane, Phys. Rev. A **48**, R4051 (1993).

[78] X. M. Tong and S. I. Chu, Phys. Rev. A **58**, R2656 (1998).

[79] X. Chu and S. I. Chu, Phys. Rev. A **63**, 023411 (2001).

[80] X. Chu and S. I. Chu, Phys. Rev. A **63**, 013414 (2001).

[81] C. Canuto, M. Y. Hussaini, A. Quarteroni, and T. A. Zang, *Spectral Methods in Fluid Dynamics* (Springer, Berlin, 1988).

[82] D. E. Ramaker and J. M. Peek, At. Data **5**, 167 (1973).

[83] M. D. Feit, J. A. Fleck, Jr., and A. Steiger, J. Comput. Phys. **47**, 412 (1982).

[84] X. M. Tong and S. I. Chu, Phys. Rev. A **61**, 021802 (2000).

[85] C. K. Chui, *An Introduction to Wavelets* (Academic, New York, 1992).

[86] P. R. T. Schipper, O. V. Gritsenko, S. J. A. Gisbergen, and E. J. Baerends, J. Chem. Phys. **112**, 1344 (2000).

[87] X. Chu and S. I. Chu, Phys. Rev. A **64**, 063404 (2001).

[88] S. I. Chu, Adv. At. Mol. Phys. **21**, 197 (1985).

[89] S. I. Chu, Adv. Chem. Phys. **73**, 739 (1989).

[90] S. I. Chu, in *Multiparticle Quantum Scattering with Applications to Nuclear, Atomic, and Molecular Physics*, edited by D. G. Truhlar and B. Simon (Springer, New York, 1997), p. 343.

[91] S. I. Chu and D. Telnov, Phys. Rep. **390**, 1 (2004).

[92] D. Telnov and S. I. Chu, Chem. Phys. Lett. **264**, 466 (1997).

[93] D. A. Telnov and S. I. Chu, Int. J. Quantum Chem. **69**, 305 (1998).

[94] D. A. Telnov and S. I. Chu, Phys. Rev. A **58**, 4749 (1998).

[95] D. A. Telnov and S. I. Chu, Phys. Rev. A **66**, 043417 (2002).

[96] D. A. Telnov and S. I. Chu, Phys. Rev. A **63**, 012514 (2001).

[97] L. J. Bartolotti, Phys. Rev. A **24**, 1661 (1981).

[98] B. M. Deb and P. K. Chattaraj, Phys. Rev. A **39**, 1696 (1989).

[99] A. K. Roy and S. I. Chu, Phys. Rev. A **65**, 043402 (2002).

[100] A. K. Roy and B. M. Deb, in *Nonlinear Phenomena in Physical and Biological Sciences*, edited by S. K. Malik *et al.* (INSA, New Delhi, 2000), p. 947.

[101] N. T. Maitra, K. Burke, H. Appel, E. K. U. Gross, and R. Leeuwen, in *Reviews of Modern Quantum Chemistry*, edited by K. D. Sen (World Scientific, Singapore, 2002), Vol. II, p. 1186.

[102] K. Capelle, G. Vignale, and B. L. Györffy, Phys. Rev. Lett. **87**, 206403 (2001).

[103] A. Nagy, Phys. Rev. A **68**, 042503 (2003).

[104] A. A. Radzig and B. M. Smirnov, *Reference Data on Atoms and Molecules* (Springer, Berlin, 1985).